Neurobiology of Disease 60 (2013) 139–151

Contents lists available at ScienceDirect

Neurobiology of Disease

journal homepage: www.elsevier.com/locate/ynbdi

Distinct phenotypes in zebrafish models of human startle disease ☆

Lisa R. Ganser [d,1], Qing Yan [a,1], Victoria M. James [b,c], Robert Kozol [a], Maya Topf [c], Robert J. Harvey [b], Julia E. Dallman [a,*]

[a] Department of Biology, Cox Science Center, 1301 Memorial Drive, University of Miami, Coral Gables, FL 33124-0421, USA
[b] Department of Pharmacology, UCL School of Pharmacy, 29-39 Brunswick Square, London WC1N 1AX, UK
[c] Institute for Structural and Molecular Biology, Department of Biological Sciences, Birkbeck College, London WC1E 7HX, UK
[d] Department of Biology and Physics, 1000 Chastain Rd, #1202, Kennesaw State University, Kennesaw, GA 30144 USA

ARTICLE INFO

Article history:
Received 29 May 2013
Revised 13 August 2013
Accepted 1 September 2013
Available online 9 September 2013

Keywords:
glra1
glrb
Glycine receptor
Startle disease
Hyperekplexia
Zebrafish

ABSTRACT

Startle disease is an inherited neurological disorder that causes affected individuals to suffer noise- or touch-induced non-epileptic seizures, excessive muscle stiffness and neonatal apnea episodes. Mutations known to cause startle disease have been identified in glycine receptor subunit (*GLRA1* and *GLRB*) and glycine transporter (*SLC6A5*) genes, which serve essential functions at glycinergic synapses. Despite the significant successes in identifying startle disease mutations, many idiopathic cases remain unresolved. Exome sequencing in these individuals will identify new candidate genes. To validate these candidate disease genes, zebrafish is an ideal choice due to rapid knockdown strategies, accessible embryonic stages, and stereotyped behaviors. The only existing zebrafish model of startle disease, *bandoneon* (*beo*), harbors point mutations in *glrbb* (one of two zebrafish orthologs of human *GLRB*) that cause compromised glycinergic transmission and touch-induced bilateral muscle contractions. In order to further develop zebrafish as a model for startle disease, we sought to identify common phenotypic outcomes of knocking down zebrafish orthologs of two known startle disease genes, *GLRA1* and *GLRB*, using splice site-targeted morpholinos. Although both morphants were expected to result in phenotypes similar to the zebrafish *beo* mutant, our direct comparison demonstrated that while both *glra1* and *glrbb* morphants exhibited embryonic spasticity, only *glrbb* morphants exhibited bilateral contractions characteristic of *beo* mutants. Likewise, zebrafish over-expressing a dominant startle disease mutation (GlyR $\alpha1^{R271Q}$) exhibited spasticity but not bilateral contractions. Since GlyR βb can interact with GlyR α subunits 2–4 in addition to GlyR α1, loss of the GlyR βb subunit may produce more severe phenotypes by affecting multiple GlyR subtypes. Indeed, immunohistochemistry of *glra1* morphants suggests that in zebrafish, alternate GlyR α subunits can compensate for the loss of the GlyR α1 subunit. To address the potential for interplay among GlyR subunits during development, we quantified the expression time-course for genes known to be critical to glycinergic synapse function. We found that GlyR α2, α3 and α4a are expressed in the correct temporal pattern and could compensate for the loss of the GlyR α1 subunit. Based on our findings, future studies that aim to model candidate startle disease genes in zebrafish should include measures of spasticity and synaptic development.

Introduction

Rhythmic motor behaviors require a balance between nervous system excitation and inhibition (E/I balance). The importance of E/I balance is illustrated by genetic mutations that selectively disrupt either excitation or inhibition and result in nervous system dysfunction (Ganser and Dallman, 2009; Gatto and Broadie, 2010). For example, in humans, startle disease/hyperekplexia results from excessive excitation due to damaging mutations in genes encoding key components of the inhibitory glycinergic synapse (Harvey et al., 2008). As the major inhibitory neurotransmitter in vertebrate hindbrain and spinal cord, glycine plays a critical role in the control of motor behaviors and reflexes. When glycinergic signaling is disrupted in newborn children, the result is exaggerated startle reflexes and hypertonia in response to unexpected auditory, tactile or visual stimuli. This abnormal startle response may also be accompanied by apnea episodes, i.e. the suspension of breathing (Thomas et al., 2010).

The majority of human startle disease cases are caused by dominant and recessive mutations in *GLRA1*, encoding the α1 subunit of the glycine receptor, GlyR α1 (Chung et al., 2010; Shiang et al., 1993; Fig. 1A). Mutations in this gene cause similar disorders in mice (Buckwalter et al., 1994; Holland et al., 2006; Ryan et al., 1994; Traka et al., 2006) and Poll Hereford cattle (Pierce et al., 2001). Dominant and recessive mutations in *SLC6A5*, encoding the presynaptic glycine transporter GlyT2, are now emerging as a second major cause of startle

* Corresponding author.
E-mail address: jdallman@bio.miami.edu (J.E. Dallman).

Available online on ScienceDirect (www.sciencedirect.com).

[1] These authors contributed equally to this work.

0969-9961/$ – see front matter © 2013 The Authors. Published by Elsevier Inc. All rights reserved.
http://dx.doi.org/10.1016/j.nbd.2013.09.002

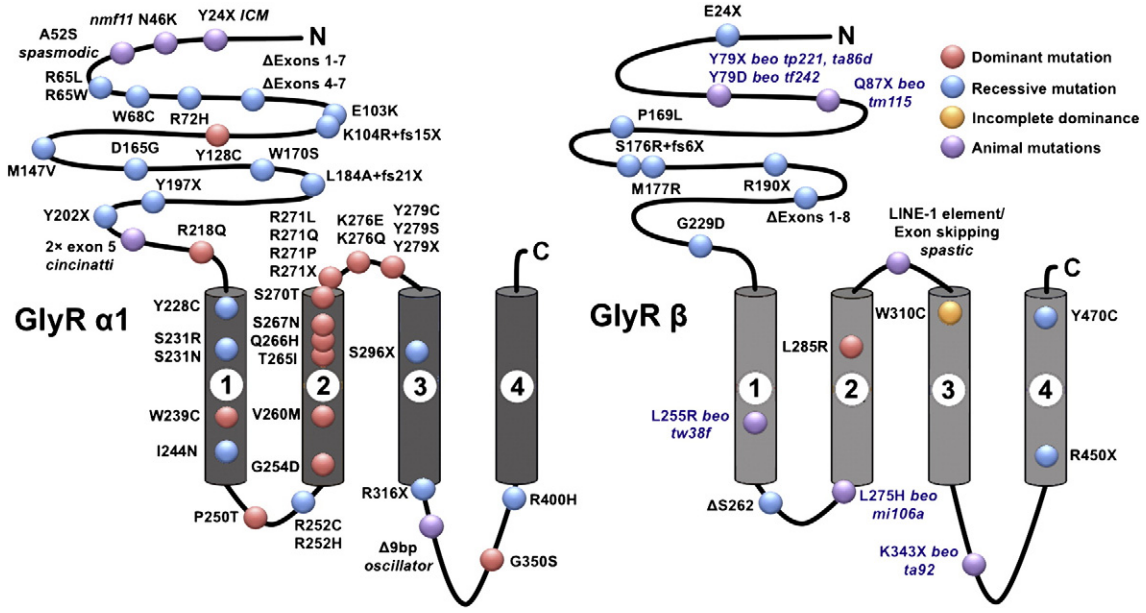

Fig. 1. Pathogenic mutations in the postsynaptic GlyR α1 and β subunits in startle disease. The predicted four-membrane spanning domain (M1–M4) topology of GlyR α1 and GlyR β subunits is depicted. Numbered columns indicate four predicted membrane-spanning domains 1–4 in each subunit. Red (dominantly inherited) and blue circles (recessively inherited) indicate the relative positions of amino acid alterations known to cause human startle disease. Purple circles indicate the relative positions of amino acid alterations found in mouse, cattle and zebrafish glycinergic disorders. For primary references to previously reported specific mutations, see Harvey et al. (2008), Chung et al. (2010, 2013) and James et al. (2013).

disease (Carta et al., 2012; Giménez et al., 2012; Rees et al., 2006), and also occur in Belgian Blue cattle (Charlier et al., 2008) and Irish wolfhounds (Gill et al., 2011). Mutations in *GLRB*, encoding the GlyR β subunit were thought to be a rare cause of human startle disease (Rees et al., 2002), although mutations in this gene were also reported in the mouse mutant *spastic* (Kingsmore et al., 1994; Mülhardt et al., 1994) and the zebrafish mutant *bandoneon* (*beo*; Granato et al., 1996; Hirata et al., 2005). However, several recent reports have identified novel dominant and recessive mutations in *GLRB* (Al-Owain et al., 2012; Chung et al., 2013; James et al., 2013; Lee et al., 2013; Fig. 1B), often associated with additional phenotypic consequences, including gaze disorders, apnea episodes, learning difficulties and developmental delay. Since GlyR α1 and β subunits occur in the same pentameric GlyR complex, it is currently unclear why mutations in *GLRB* can give rise to a more severe clinical phenotype than mutations in *GLRA1*.

To model human startle disease, zebrafish are an attractive model because genes can be 'inactivated' using antisense morpholino knockdown (Eisen and Smith, 2008). Moreover, the resulting swimming phenotypes are readily quantified (Burgess and Granato, 2007). In contrast to mammalian genomes with five known GlyR subunit genes (*GLRA1*, *GLRA2*, *GLRA3*, *GLRA4* and *GLRB*), the zebrafish genome encodes seven GlyR subunit genes (*glra1*, *glra2*, *glra3*, *glra4a*, *glra4b*, *glrba*, and *glrbb*; Hirata et al., 2010). The two duplicate genes, *glra4b* and *glrbb* resulted from whole genome duplication early in the evolution of teleosts (Hurley et al., 2007a). This phenomenon can be advantageous, since individual paired genes often differ in terms of expression patterns and functional roles (Hurley et al., 2007b; Ogino et al., 2011). For example, the zebrafish mutant *bandoneon* (*beo*) harbors mutations in one of the paired GlyR β subunit genes (*glrbb*), resulting in touch-induced simultaneous bilateral contractions of the axial muscles due to the loss of reciprocal glycinergic inhibition of motor circuits (Hirata et al., 2005, 2010). Despite the duplication of the GlyR β subunit genes in zebrafish, *glrba* is unable to compensate for the loss of *glrbb* function due to a different expression pattern, suggesting that it forms part of a distinct GlyR with a unique function (Hirata et al., 2005). Since mutations in human *GLRA1*, *GLRB* and *SLC6A5* all result in startle disease (Harvey et al., 2008), it is unusual that to date no mutations in *glra1* or *slc6a5* have been discovered that produce bilateral contractions in larval zebrafish. We therefore sequenced the remaining *beo* alleles and have confirmed that they all harbor damaging mutations affecting *glrbb*.

To directly compare zebrafish *glra1* and *glrbb* startle disease models, we designed splice-site morpholinos to knockdown the expression of these genes (Draper et al., 2001). As expected, injecting *glrbb* morpholinos produced a phenotype similar to *beo* mutants, characterized by simultaneous bilateral contractions strong enough to shorten the body. In addition, both *glrbb* and *glra1* morphants produced spastic and erratic behaviors at early stages, but in contrast to *glrbb* morphants, *glra1* morphants only rarely produced bilateral contractions and by 48 hpf *glra1* morphants produced normal behaviors. Immunohistochemistry of *glrbb* and *glra1* morphants also demonstrated distinct GlyR immunostaining patterns on early-differentiating spinal neurons. While *glra1* morphants exhibited reduced but still synaptic GlyR staining, *glrbb* morphants exhibited GlyR α subunit trapping in intracellular, non-synaptic compartments, suggesting that the more severe *beo* phenotype results from a loss of multiple GlyR subtypes. Our quantitative analysis of mRNA expression for glycinergic genes in early development identified *glra2* and *glra3* as having high expression levels early in development that could ameliorate the *glra1* morphant phenotype. In summary, we identify a phenotypic range in zebrafish startle disease models that should be taken into account when using zebrafish to study novel candidate startle disease genes.

Materials and methods

Fish care and embryo rearing

Experiments were carried out using *Danio rerio* wild type strains AB, Tubingen, and BWT (a fish store strain from Long Island). Adults were kept on a 14 hour light/10 hour dark circadian cycle at 28.5 °C. Embryos were collected from natural crossings shortly after removing a divider at first light. Embryos were then reared in glass Petri dishes containing system water (water that houses the adult fish) in a 28.5 °C incubator with the same 14 hour light/10 hour dark cycle. All experiments were

conducted in accordance with the University of Miami Institutional Animal Care and Use Committee guidelines.

Detection of beo mutations

DNA was extracted from fin clips of *beo* mutation carriers using a QIAamp DNA mini kit (Qiagen, Manchester, UK). The nine coding exons and flanking sequences of *glrbb* were amplified from purified genomic DNA. Forward and reverse primers each of 20–30 bp in length were designed to cover the start and end of the regions to be amplified and ordered from Eurofins MWG Operon (Ebersberg, Germany). DNA polymerase was ordered from Clontech, Saint-Germain-en-Laye, France. PCR products were gel purified and cloned into pCR4-TOPO (Invitrogen, Paisley, UK). Sanger sequencing was performed by the DNA Sequencing Service (University of Dundee, UK). DNA sequences were analyzed using Sequencher 5.1 software (GeneCodes Corporation, Ann Arbor, USA) by alignment with reference sequences downloaded from NCBI or UCSC databases. For mutation identification, single nucleotide variants (SNVs) were noted and the effect of these changes on the encoded protein were examined using bioinformatics software including SIFT (Kumar et al., 2009) and Polyphen-2 (Adzhubei et al., 2010).

Morpholino design and injection

Splice site-targeted morpholinos (MOs) were designed against *glra1* and *glrbb*. Intron/exon junctions were selected for MO design based both upon the appropriateness of the sequence for effective MO knockdown (i.e. 50% GC content and multiple mismatches to related genes). Two distinct MOs against *glra1* were tested to control for possible off-target effects: *glra1*MOex4 5′-GAATTGTCCTCTCACCTTATACTGT-3′ and *glra1*MOex7 5′-CTTCCCTGAAACACAGAGAGTATGT-3′. Off-target effects were not a concern in the case of the *glrbb* splice morpholino *glrbb*MOex5 5′-GAGAGCATTAAAGTTCACCTCATGC-3′ because of the previously described *beo* mutant phenotype (Hirata et al., 2005). For control-injected embryos, we used the standard control MO provided by Gene Tools (Gene Tools, LLC; Philomath OR). Lyophilized MOs were resuspended in water as 1 mM stocks and stored at room temperature. Prior to use, the MO stock solution was heated for 5 min to 65 °C. For injection, stock solutions were diluted in a filtered solution of 1% (w/v) fast-green dye. MOs were injected using filament-lined Kwik-Fil borosilicate capillary glass (World Precision Instruments, Sarasota FL) pulled on a P-97 micropipette puller (Sutter Instruments, Novato CA) to a long taper with a fine tip that was broken back to ~1 μm using forceps. A stage micrometer was used to calibrate the injection rig to produce a 100 μm diameter bolus. MOs were injected into wild type embryos at the 1–2 cell stage. Embryos were sorted 6–8 h after injection so that only morphants in which the MO bolus had evenly dissipated were later analyzed for behavioral phenotypes.

RT-PCR

Unless otherwise stated, all reagents were from Life Technologies, Grand Island NY. Once behavioral analyses were completed, embryos were ground in TRIzol for RNA extraction. RNA preparations were then DNase-treated using DNA-free. The reverse transcriptase SuperScript III with either an anchored oligo(dT) primer or a gene specific primer was used to synthesize cDNA for subsequent PCR analysis. Diagnostic PCR primers were designed to detect mis-splicing events induced by MO masking of intron/exon junctions for *glra1* (Fex3 5′-TTGGATCC ATTGCTGAAACA-3′; Rex8 5′-ATACTCCAGCAGGGCAGAGA-3′) and *glrbb* (Fex5 5′-CTGAGACAACGCTGGAATGA-3′; Rex8 5′-CTCCACGCACGTG TAGTAGC-3′) (All primers were synthesized by Integrated DNA Technologies, Coralville, IA). Primers targeting *slc6a5* (F: 5′-AG GAGTCACTCTGCCTGGAG-3′; R: 5′-CAAATGCAATTCCTGGACCT-3′) were utilized as internal controls. Shifted RT-PCR products caused by MO-induced alterations in pre-mRNA splicing were gel purified using Wizard Gel and PCR Clean-up System (Promega, Madison, WI). Purified bands were then re-amplified and sequenced using Sanger DNA sequencing to determine the predicted impact on targeted proteins.

Behavioral analyses

A high-speed camera (1024 Photron FASTCAM, San Diego, CA) was used to record spontaneous and touch-evoked behaviors of 17 to 50 hpf control, *glra1*, and *glrbb* morphants. Embryos were manually dechorionated. Spastic behaviors were characteristic of all groups just after dechorionation. Therefore, behavioral assays were conducted at least 1 h after dechorionation. Videos were scored by hand to generate ethograms that highlight rhythmic and spastic aspects of behaviors.

Immunohistochemistry

Cryosectioning and antibody staining were performed as previously described (Ogino et al., 2011). Briefly, anesthetized fish embryos were embedded in O.C.T. compound (Tissue-Tek, Torrance, CA) and gradually frozen in liquid nitrogen. Samples were then sectioned on a cryostat (CM-1850, Leica) and mounted on poly-L-lysine coated slides (Newcomer Supply, Middleton, WI) prior to a 10 min fixation in 4% (w/v) formaldehyde (diluted from 16%, Pierce Biotechnology, Rockford, IL). Anti-gephyrin (clone mAb7a, mouse IgG1, 1:500, Synaptic Systems, Göttingen, Germany), and a pan anti-GlyR α subunit (clone mAb4a, mouse IgG1, 1:100, Synaptic Systems) were used as primary antibodies. Alexa 488- and Alexa 568-conjugated donkey anti-mouse IgGs were used as secondary antibodies (1:2000, Life Technologies, Carlsbad, CA). Double staining with anti-gephyrin and anti-GlyR α subunit antibodies was performed sequentially. Stained sections were mounted in Vectashield/DAPI (Vector Laboratories, Burlingame, CA) and images were captured on a confocal microscope using a 1.4 NA 63× oil objective (SP5, Leica Wetzlar Germany).

Quantification of synaptic staining

Images were processed using ImageJ (NIH). The brightness and contrast were adjusted to maximize dynamic range and reduce background noise before analyzing the density of GlyR α subunit and gephyrin puncta. For puncta density analysis, to avoid the impact of variation along the anterior–posterior axis, three images were picked in each stack: one each near top, middle, and the bottom of the stack. The area with puncta expression in each image was calculated in ImageJ. GlyR α subunit and gephyrin puncta in each image were identified and counted by custom MatLab (MathWorks, Natick, MA) programs (Morgan et al., 2008; Soto et al., 2011). For GlyR α subunit and gephyrin puncta co-localization analysis, puncta in the three-dimensional stack were first found by custom MatLab programs (Morgan et al., 2008; Soto et al., 2011). Then the three-dimensional location of each voxel in all GlyR α subunit puncta and gephyrin puncta were compared in MatLab to identify the colocalized puncta.

Quantitative PCR

Primers were designed against genes associated with the glycinergic synapse (Table 1). Primers were designed using Primer3 (Rozen and Skaletsky, 2000) to span introns with the goal of excluding the possibility that residual genomic DNA contributed to estimates of transcript abundance. To generate a developmental time series, RNA from 24, 32, 48 and 72 hpf wild type embryos was harvested. RNA extraction method followed the manufacturer's protocol (TRIzol, Life Technologies, Carlsbad, CA). Extracted RNAs were then DNase-treated (DNA-Free, Life Technologies), quantified on a NanoDrop 2000 (ThermoScientific,

Table 1
Oligonucleotide primers used for RT-PCR analysis. Key for selected gene names: *slc6a5* encodes GlyT2, *slc6a9* encodes GlyT1, *slc32a1* encodes VGAT/VIAAT, and *eef1a1l1* encodes the housekeeping protein EF1.

Gene	Oligonucleotides	T_m	Size (bp)	Ensembl protein ID
glra1	F: GGATCTCGAGCCTCTCTTCC	57	67	ENSDARP00000136733
	R: CACACTGCCATCCAAATGTC	54		
glra2	F: CGTGGTCAAAAACACACAGG	55	115	ENSDART00000066192
	R: GCGTGATATGGTGTCGATTC	54		
glra3	F: CCTGATCTTTGAGTGGCAAG	54	116	ENSDARP00000009777
	R: TGTTGTAGTGCTTGGTGCAG	56		
glra4a	F: GCAGCACAAGGAGTTCATCA	56	90	ENSDARP00000146445
	R: TCCGTACCCTCGGAAGTAAA	55		
glrba	F: CCGGAAAACCACAGAACAAG	54	112	ENSDARP00000074685
	R: AACGTGAAAGGGAACAGAGC	55		
glrbb	F: TGCTCATCATCTGTCTGTGG	55	73	ENSDARP00000127692
	R: CCTTTCTTCTTTCCCTTTTTAGC	52		
gphna	F: GCCCACCATCATCAAAGC	54	65	ENSDARP0000087952
	R: GATGGTACTCTGGACGTGGA	56		
gphnb	F: TCAGCAGCAGACTGATGAGC	57	85	ENSDARP00000005053
	R: TTGTGCAGCTCCACGTATTG	56		
slc6a5	F: GGATTCCCATCATGTTTGCT	53	87	ENSDARP00000071929
	R: CGGGTTGAGGAGAACATACC	55		
slc6a9	F: AAGATTGCCATGTCTGAAGGA	54	65	ENSDARP00000088755
	R: GGTCGGGTTTCACAGAGTTC	55		
slc32a1	F: ACAAGCCCAGAATCACTGCT	57	95	ENSDARP00000083453
	R: GTGGAGAATGGCGTAGGGTA	56		
eef1a1l1	F: CTGGAGGCCAGCTCAAACAT	58	82	ENSDARG00000020850
	R: ATCAAGAAGAGTAGTACCGCTAGCA	58		

West Palm Beach, FL) and electrophoresed on a 1% (w/v) agarose gel to assess quality.

The SuperScript III First-Strand Synthesis System (Life Technologies, Carlsbad CA) was used for cDNA synthesis. However, gene specific primers (GSPs) were used in place of oligo(dT) to better detect rare transcripts encoding synaptic proteins. Each synthesis reaction contained 1 μg of RNA template. To generate standard curves, serial dilutions of gel-purified PCR products were used as template. Products were purified using the Wizard SV Gel and PCR purification kit (Promega, Madison WI). Stocks were made from a 1:1000 dilution of purified PCR product in DNase/RNase free H_2O. Serial dilutions were adjusted to encompass the range of expression levels for each gene. qPCR reactions contained 2 μL of RNase/DNase free H_2O, 14.5 μL Master mix, 2.5 μL of 10 mM primer and 1 μL of cDNA template at a final volume of 20 μL. The PCR protocol was as follows: 1 step of 95 °C for 5 min; 30 cycles of 95 °C for 30 s, 55 °C for 30 s, 72 °C for 30 s; and 1 step of 72 °C for 1 min. For qPCR, we used an Eppendorf Mastercycler ep realplex4 with the realplex 1.5 software using a Twin Tec Semi-Skirted 96 well plate. Each well contained 5 μL of PerfeCTa SYBR Green FastMix (Quanta BioSciences, Gaithersberg MD), 1.5 μL 10 mM combined forward and reverse primer, 2.5 μL of H_2O and 1 μL of cDNA template to a final volume of 10 μL. The PCR protocol was as follows: 1 step of 95 °C for 1 min; 40 cycles of 95 °C for 15 s, 55 °C for 20 s, 68 °C for 30 s; and a melting curve and a final step of 95 °C. Three samples of each time point were run in duplicate on the same plate with a standard curve consisting of four 1:10 serial dilutions of purified PCR product as template. Relative mRNA copy numbers were calculated based on the expression levels of the housekeeping gene encoding EF1 (Tang et al., 2007).

Results

Sequencing of additional beo mutants confirms that mutations are found exclusively in glrbb

Mutations in *glrbb* were previously identified as the basis for the *beo* mutant phenotype (Hirata et al., 2005). In the original study, the underlying mutations for some, but not all *beo* alleles were identified (Hirata et al., 2005; Table 2). These resulted in either missense (*tw38f*, p.L255R in TM1, *mi106a*, p.L275H in TM2) or nonsense (*tp221*, p.Y79X) mutations. Since *glra1* and *glrbb* genes are both located on zebrafish chromosome 14 and participate in the same GlyR complex, we speculated that some of the remaining *beo* alleles might actually be mutations in *glra1* that could fail to complement mutations in *glrbb* due to linkage. To determine the types of mutations in remaining *beo* alleles *ta86d*, *ta92*, *tm115* and *tf242*, we obtained these lines from the zebrafish Stock Center in Tübingen, Germany. We first amplified the nine coding exons of *glrbb*, which revealed unique missense mutations (*tf242*, c.T301G, p.Y79D) or nonsense mutations resulting in premature termination of the GlyR βb polypeptide (*ta86d*, c.T303A, p.Y79X; *tm115*, c.C325T, p.Q87X and ta92, c.A1093T, p.K343X respectively; Fig. 1, Table 2). It is also noteworthy that both *tp221* and *ta86d* alleles harbor the same mutation — p.Y79X. Since the remaining *beo* allele, *tu230*, was lost (Granato et al., 1996), we conclude that all available *beo* alleles harbor mutations in *glrbb*.

Splice site-targeted morpholino knockdown of glra1 and glrbb genes

Given that all available *beo* alleles can be explained by mutations in *glrbb*, we investigated the phenotype resulting from *glra1* inactivation in zebrafish. Two independent, splice site-targeted morpholinos (MOs), *glra1*MOex4 and *glra1*MOex7, were designed

Table 2
Mutations identified in *beo* mutant alleles. SNVs that result in nonsense mutations (p.Y79X, p.Q87X and p.K343X) will lead to a truncated and incomplete proteins, leading to a deleterious phenotype. While ta86d, tp221, and tm115 mutations will truncate the protein close to the N-terminus (p.Y79X or p.Q79X) creating a small non-functional GlyR βb subunit, the viable ta92 allele (p.K343X) will truncate the GlyR βb subunit within the long intracellular loop between transmembrane helices M3 and M4. Notably, the M3–M4 loop is critical for binding gephyrin, which clusters the GlyRs at synapses. Since the gephyrin-binding site on the GlyR βb subunit is predicted to reside between amino acids 396 and 413 (Hirata et al., 2005), truncation of GlyR βb subunit at residue 343 would result in a truncated protein lacking the gephyrin binding site and the fourth membrane-spanning domain (M4). However, the N-terminal extracellular domain and M1–M3 would be intact. This perhaps explains why ta92 is the only viable *beo* allele. Missense mutations in alleles tf242, tw38f and mi106a, resulting in p.Y79D, p.L255R and p.R275H substitutions were analyzed using the bioinformatics packages SIFT and Polyphen-2, which predicted these amino acid substitutions to be deleterious or probably damaging, respectively.

beo allele	cDNA	Substitution[d]	Consequence	SIFT	Polyphen-2	Reference
tu230[a]	Allele lost	–	–	–	–	Hirata et al. (2010)
tp221[c]	c.T303A	p.Y79X	Truncation	–	–	Hirata et al. (2005)
tm115	c.C325T	p.Q87X	Truncation	–	–	This study
tf242	c.T301G	p.Y79D	Missense	Deleterious (<0.05)	Probably damaging (1.00)	This study
ta92[b]	c.A1093T	p.K343X	Truncation	–	–	This study
tw38f	c.T830G	p.L255R	Missense	Deleterious (<0.05)	Probably damaging (1.00)	Hirata et al. (2005)
ta86d	c.T303A	p.Y79X	Truncation	–	–	This study
mi106a	c.G990A	p.R275H	Missense	Deleterious (<0.05)	Probably damaging (1.00)	Hirata et al. (2005)

[a] Mutant lost.
[b] Viable allele.
[c] Strongest allele.
[d] Amino acid co-ordinates correspond to the mature GlyR βb subunit polypeptide after signal peptide cleavage.

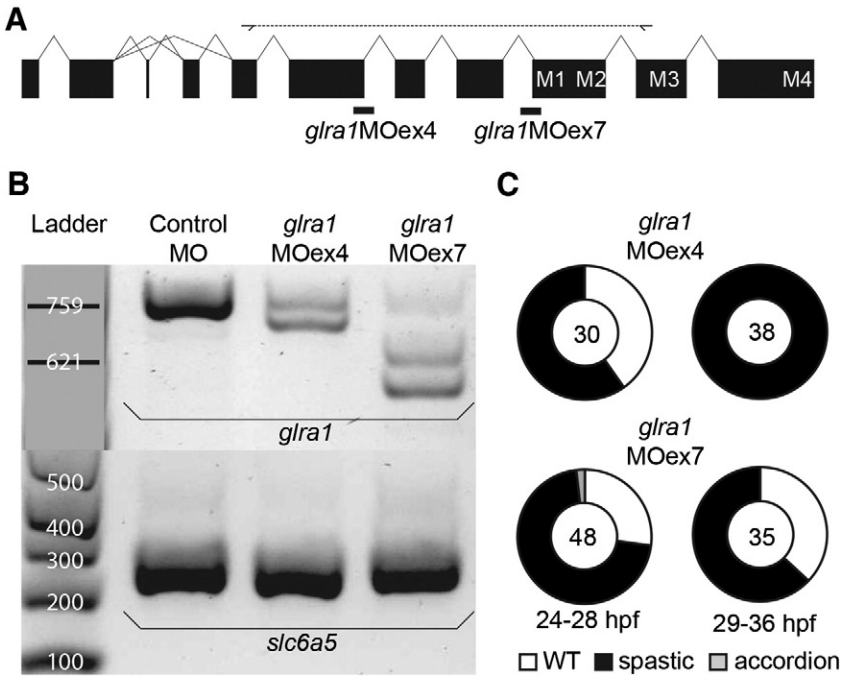

Fig. 2. Efficacy and target specificity of splice-site-blocking *glra1*ex4 and *glra1*ex7 morpholinos. A. Schematic representation of the zebrafish GlyR α1 subunit gene (*glra1*). Exons, shown as black boxes, are connected by introns, shown as lines. Two of the exons, 2a and 2b, are alternatively spliced as indicated by multiple possible intron lines. Exons that encode membrane-spanning domains M1–M4 are indicated. Two distinct splice-site-blocking MOs (thick black bars) were designed to knock down *glra1* expression by masking exon/intron junctions. Exon4/intron4 is masked by *glra1*MOex4, and intron6/exon7 by *glra1*MOex7. Diagnostic primers were designed to amplify exons 3 to 8 to detect MO-induced mis-splicing events. B. RT-PCR results demonstrate specificity of altered *glra1* pre-mRNA splicing caused by MO injection. The leftmost lane contains two size standards that replace the ladder and are based on direct Sanger sequencing of the bands. The following two lanes contain RT-PCR of RNA samples from 28 hpf embryos injected with 2 nL 0.5 mM control MO, 2 nL 0.25 mM *glra1*MOex4, and 2 nL 0.5 mM *glra1*MOex7 respectively. In the upper gel, *glra1* diagnostic primers are used for PCR from cDNA synthesized using a gene-specific primer for *glra1*. In contrast to control morphants that show a single strong PCR product at 759 bp, *glra1*MOex4 morphants exhibit reduced levels of the wild type PCR product and a new product of 698 bp, indicating exon skipping. Likewise, *glra1*MOex7 morphants exhibit reduced levels of the wild type PCR product and two PCR products of 621 and 544 bp in size. In the lower gel, PCR for a GlyT2 cDNA (*slc6a5*) is used as a loading control, and is amplified from cDNA synthesized using anchored oligo-dT primers. C. Percentages of *glra1*MOex4 and *glra1*MOex7 morphants exhibiting wild type (wt), spastic or accordion phenotypes, plotted at 24–28 hpf and 29–36 hpf. The number of embryos analyzed is indicated at the center of each plot.

against intron/exon boundaries shared among all *glra1* transcripts (Fig. 2A). The *glra1*MOex4 targets the 3′ acceptor site of exon 4, an exon that encodes determinants of glycine binding (Lynch, 2004; as well as the epitope recognized by the anti-GlyR antibody mAb4a) while *glra1*MOex7 targets the 5′ donor site of exon 7 that encodes the first two membrane-spanning domains (M1 and M2) of the GlyR α1 subunit. Both MOs would be expected to disrupt GlyR function by causing exon-skipping or intron-retention, introducing a frameshift, and truncating translated proteins. RT-PCR analysis of RNA harvested from 28 hpf *glra1* morphants revealed the nature of mis-splicing events induced by MO injections. Diagnostic primers were designed to detect both exon-skipping and intron-retention events and morphant-specific bands were subsequently gel purified and sequenced to determine the exact nature of the MO-induced disruption (Eisen and Smith, 2008). For *glra1*MOex4, we identified a single morphant band caused by a 61 bp deletion due to a cryptic-splice-donor site towards the 3′ end of exon 4 (Fig. 2B; middle lane). For *glra1*MOex7, we identified two morphant-specific PCR products, both smaller than the wild type product (Fig. 2B; right-most lane). Sequencing of *glra1*MOex7 morphant-specific bands demonstrated that the lower of the PCR products is a result of skipping exon 7 entirely, while the middle band is the result of a cryptic splice-site in the middle of exon 7. The cryptic splice-site results in an in-frame transcript. Nonetheless, the resulting protein would still be expected to lack function because of deletion of the transmembrane domain M1.

Although a translation-blocking MO had previously been designed to knock down *glrbb* (Hirata et al., 2005), this MO did not work in our hands, possibly due to sequence variability surrounding the start methionine in different wild-type strains. In addition, we cannot monitor the efficacy of this translation-blocking MO, due to the lack of a specific GlyR βb antibody. Therefore, we designed a new splice-site morpholino against 3′ acceptor site of *glrbb* exon 5, one of the largest exons upstream of the transmembrane domains (Fig. 3A). Using *glrbb*MOex5, we were able to faithfully recapitulate the *beo* mutant accordion phenotype resulting from tonic bilateral muscle contractions (Fig. 3D). RT-PCR analysis of RNA harvested from *glrbb*MOex5-injected embryos at 28 hpf demonstrates that *glrbb*MOex5 caused a 156 bp deletion and sequencing this PCR product demonstrated that a cryptic splice-donor site in exon 5 accounted for morpholino-induced mis-splicing (Fig. 3B; right lane).

Quantification of the onset of swimming behavior

From 24 to 36 hpf, zebrafish larvae transition from coiling behaviors (not propulsive) to rhythmic alternating motor behaviors that can propel the larva away from a threat (Saint-Amant and Drapeau, 1998). Therefore analysis of morphant behaviors at these stages occurs against a rapidly changing but highly stereotyped control baseline. To quantify behaviors, we determined the duration of discrete components of two, sequential touch-induced behaviors in each larva (Fig. 4). For example, in response to touch, a control morphant coils in one direction (light blue bar) until tail touches head (black column), coils in the opposite direction (dark blue bar) until tail touches head (black column) and slowly returns to rest (tan bar). While the exact timing of the two independent behaviors varies, the sequence of components is the same. To capture the developmental progression of control morphant behaviors from 24 to 36 hpf, we plotted single behaviors for 50 individual larva that span the behavioral transition from coiling to propulsive swimming (Fig. 5; left column). We split the 24–36 hpf time period into two qualitatively distinct early, 24–28 hpf, and late, 29–36 hpf bins. Staging is

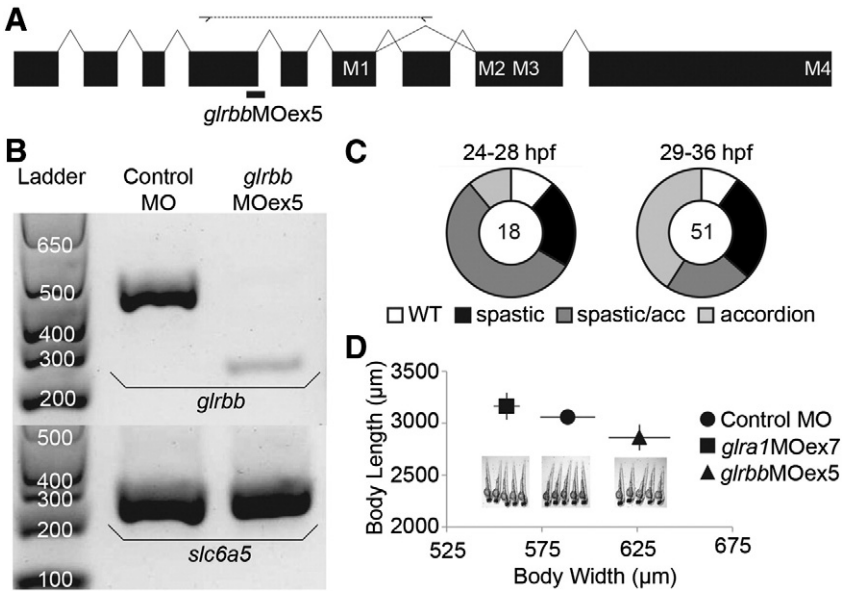

Fig. 3. Efficacy and target specificity of splice-site-blocking *glrbb* exon 5 morpholinos. A. Schematic representation of the zebrafish GlyR βb subunit gene (*glrbb*). Exons, shown as black boxes, are connected by introns, shown as lines. Exons that encode membrane-spanning domains M1–M4 are indicated. The *glrbb*MOex5 splice-site-blocking MO (thick black bar) was designed to knockdown *glrbb* expression by masking exon/intron junction intron4/exon5. Diagnostic primers designed to amplify exons 5 to 8 were used to detect MO-induced mis-splicing events. B. RT-PCR results demonstrate specificity of altered *glrbb* pre-mRNA splicing caused by MO injection. The leftmost lane contains a size standard ladder followed by two lanes of RT-PCR from RNA samples of 28 hpf embryos injected with 2 nL 0.5 mM control MO and 2 nL 0.5 mM *glrbb*MOex5 respectively. In the upper gel, *glrbb* diagnostic primers are used for PCR from cDNA synthesized using a gene-specific primer for *glrbb*. In contrast to control morphants, where a single strong PCR product of 430 bp is detected, *glrbb*MOex5 morphants exhibit reduced levels of the wild type PCR product and a new product of 274 bp, indicating exon skipping. In the lower gel, PCR for a GlyT2 cDNA (*slc6a5*), amplified from cDNA synthesized using anchored oligo-dT primers, is used as a loading control. C. Percentages of *glrbb*MOex5 morphants exhibiting wild type (wt), spastic or accordion phenotypes are plotted at 24–28 hpf and 29–36 hpf. The number of embryos analyzed is indicated at the center of each plot. D. Pictures of 5 representative 48 hpf larvae demonstrate shortening of the body axis produced by tonic bilateral contraction in *glrbb* but not *glra1* morphants. Length and width (yolk to back) measurements (average n = 5, error bars indicate standard deviation). A Student's t-test indicates that *glrbb* morphants are significantly shorter ($p < 0.05$) and wider ($p < 0.005$) than their control and *glra1* morphant counterparts.

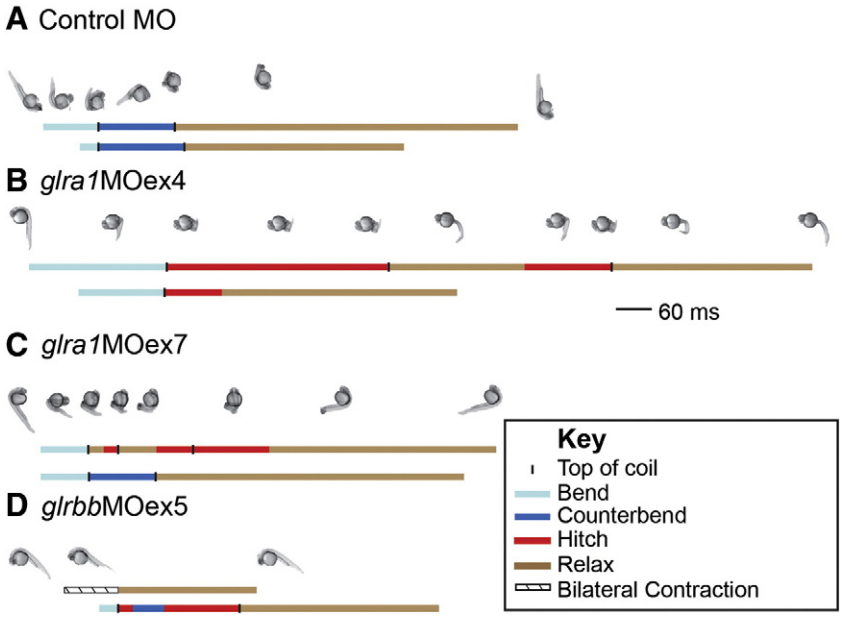

Fig. 4. Repeated stimulation evokes erratic, sometimes spastic behaviors in *glra1* and *glrbb* morphants. Two sequential, touch-evoked behaviors are plotted for four, representative morphant larvae: control, A; *glra1*MOex4, B; *glra1*MOex7, C; and *glrbb*MOex5, D. Behaviors were recorded using a high-speed camera and plotted as lines with the different behavioral components indicated by line color and each component's duration indicated by line length (scale bar = 60 ms; light blue = initial bend; dark blue = counter-bend; black column = top of coil, when the tail comes closest to touching the head; tan = return to rest; red = stuck or bend to same side; boxed diagonal lines = bilateral contraction). Still frames are included above the first of two plots with the number of pictures/length reflecting relative rates of change in the movement. A. The control morphant exhibited behavioral stereotypy with repeat stimulation: both behaviors consist of two coils in alternating directions followed by relaxation. B. The *glra1*MOex4 morphant exhibited erratic, spastic behaviors. In the first behavior, the *glra1*MOex4 morphant produced spastic behavior, getting stuck in the first coil and producing a second coil to the same side as the first. The second behavior was different from the first-the *glra1*MOex4 larva produced only one coil, and still spastic-the larva got stuck in the coil. C. The *glra1*MOex7 morphant also exhibited erratic, spastic behaviors. In the first behavior, the *glra1*MOex7 larva produced three coils, all to the same side. The second behavior was different from the first—this behavior was not spastic, consisting of two smooth alternating coils that return to rest. D. The *glrbb*MOex5 morphant larvae exhibited erratic, bilateral contraction and spastic behaviors. In the first behavior, the *glrbb*MOex5 morphant produced bilateral contraction that actually shortened the body axis–the classic accordion phenotype. The second behavior was different from the first—this time the *glrbb*MOex5 morphant produced two coils, getting stuck in each of these coils.

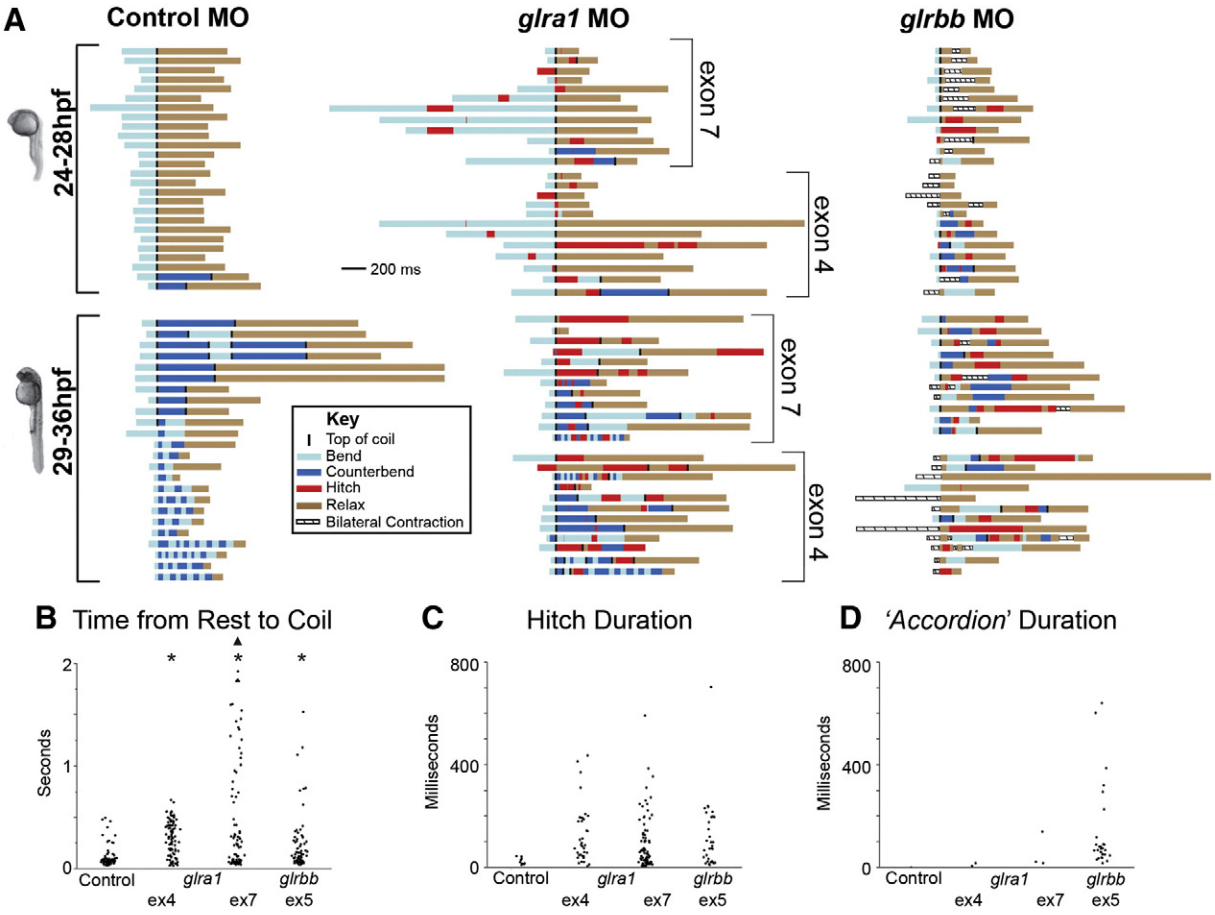

Fig. 5. Spasticity is characteristic of both *glra1* and *glrbb* morphants but bilateral contraction mainly occurs in *glrbb* morphants. A. One behavior per larva is plotted for representative populations of 50 control (left column), 48 *glra1* (middle column), and 47 *glrbb* (right column) morphants that span the 24–36 hpf time period. All larvae were stimulated twice but only one of each pair of behaviors was plotted here. (Scale bar = 200 ms; light blue = initial bend direction; dark blue = counterbend; black column = top of coil, when the tail comes closest to touching the head; tan = return to rest; red = stuck or bend to same side; boxed diagonal lines = bilateral contraction). Larval staging was based on using the angle of the head to the long tail axis as diagnostic of stage (Kimmel et al., 1995). B. Time from rest to first coil is plotted for all recorded control (n = 83), *glra1*ex4 (n = 92), *glra1*ex7 (n = 92), and *glrbb*ex5 (n = 68) morpholino-injected larvae. ANOVA indicated a significant effect of morpholino injected on time to first coil [$F(3,334) = 15.8225$, $p = 0.0001$]. Post hoc Bonferroni-corrected Student's t-tests compared all means and showed significant differences at $p < 0.05$ (*) that both *glra1* morphants and *glrbb* morphants are significantly different from control morphants. In addition, *glra1*ex7 morphant times to first coil were significantly longer ($p < 0.05$, black triangle) than *glra1*ex4 and *glrbb*ex5 morphants. C. Hitch durations in milliseconds are plotted for any of the control, *glra1*, or *glrbb* larva that exhibited this behavior. ANOVA indicated no significant effect of morpholino injected on hitch time [$F(3,155) = 2.41$, $p = 0.07$], thus there is no subsequent post hoc analysis. D. 'Accordion' durations in milliseconds are plotted for any of the control, *glra1*, or *glrbb* larva that exhibited this behavior. The 'accordion' behavior is clearly more frequent in *glrbb*ex5 morphants, occurring 27 times compared to never in controls and 5 times in all *glra1* morphant larvae.

based on a two criteria: time in hpf and morphology (Kimmel et al., 1995). Single coils first transitioned to alternating coils, 24–28 hpf, and then, 29–36 hpf, to swimming characterized by shallower and more rapid alternating bends (Fig. 5; left column).

glra1 and glrbb morphants exhibit spasticity

Both *glra1* and *glrbb* morphants exhibit spastic and erratic behaviors during 24–36 hpf (Figs. 2C & 3C). Spastic behaviors (indicated by red bars) were characterized by hitches. We defined hitches as pauses that disrupted the smooth progression of a movement and/or repeated bends to one side (Figs. 4B, C & D; Fig. 5, middle & right columns). Behaviors were also erratic, lacking stereotypy when elicited multiple times (Supplemental movies; Figs. 4B, C & D). In addition, the duration of the time to first coil was significantly longer in *glra1* morphants (*glra1*MOex4: 296 ± 18 ms, n = 93; *glra1*MOex7: 444 ± 56 ms, n = 93) and *glrbb* morphants (*glrbb*MOex5: 241 ± 33 ms, n = 69) compared to control morphants (Control MO: 109 ± 11 ms, n = 83, means ± standard deviation for all treatments; Fig. 5B). Spasticity in both *glra1* and *glrbb* morphants (Fig. 5C) was associated with a delay in the onset of rhythmic behaviors seen in control morphants at 30–36 hpf. In addition to spasticity, *glrbb* morphants exhibited simultaneous bilateral contractions strong enough to shorten the body axis–the diagnostic accordion phenotype (Granato et al., 1996; Figs. 3D, 4D & 5D; Supplemental movies). Moreover, in contrast to *glra1* morphants in which behavioral disruptions were transient, *glrbb* morphant phenotypes persisted, resulting in larvae with a shortened axis by 48 hpf (Fig. 3D). Spastic phenotypes were recapitulated by injecting mRNA encoding a dominant-negative GlyR α1 subunit mutant R270Q (Figs. 6B & C). Curiously, by contrast to the dominant-negative *glra1* R270Q RNA that lacked a morphological phenotype, over-expressing the wild type GlyR α1 subunit mRNA produced shortened-axis and Cyclops phenotypes (Figs. 6A & C). Cyclopic phenotypes are commonly associated with disrupted *sonic hedgehog* (shh) signaling in early embryos and likely reflect the disruptive effect of mis-expressing functional glycine receptors.

glrbb is epistatic to glra1 at the level of behavior

To formally test for epistatic relationships between *glra1* and *glrbb*, we co-injected *glrbb*MOex5 with wither *glra1*MOex4, *glra1*MOex7, or control morpholinos and analyzed the resulting phenotypes (Table 3).

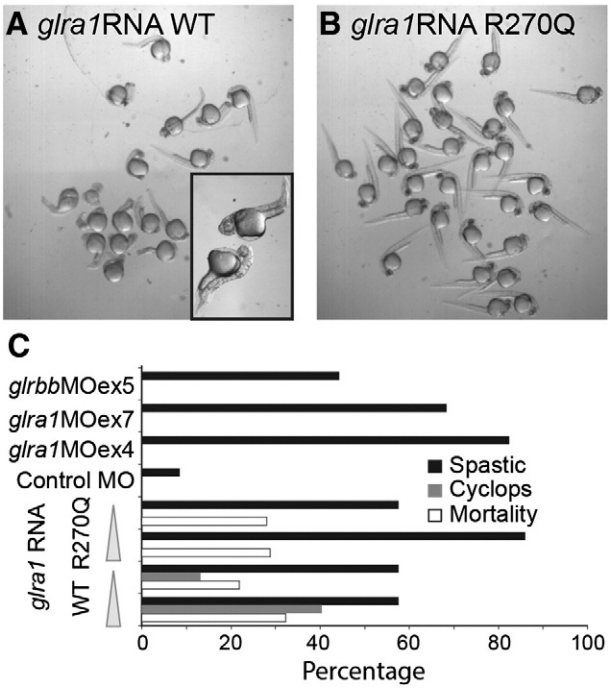

Fig. 6. Injection of dominant-negative GlyR α1 subunit R270Q mutant RNA recapitulates *glra1* morphant spasticity. A, B. Populations of 30 hpf larvae were injected as zygotes with ~2 ng of either wild type, A, or R270Q dominant-negative *glra1* RNA, B. While R270Q *glra1* RNA-injected larvae were morphologically normal, surprisingly, 60% of wild type *glra1* RNA-injected larvae exhibited shortened axis and cyclopic phenotypes. These phenotypes are more commonly associated with defects in early signaling through the *sonic hedgehog* pathway and are likely a consequence of expressing functional glycine receptors at a time when they are not normally expressed. In A, boxed inset, it is possible to see the medially fused eyes characteristic of the Cyclops phenotype. C. Percentages of larvae from different treatment groups that exhibited spastic or Cyclops phenotypes or mortality are plotted. RNAs encoding wild type and GlyR α1 subunit R270Q mutant were each injected at two concentrations indicated by the wedge (wt high ~2 ng, n = 25; low ~400 pg, n = 23; R270Q high ~2 ng, n = 42; low ~400 pg, n = 17).

Embryos co-injected with *glrbb* and *glra1* morpholinos exhibited the classic accordion phenotype of bilateral muscle contractions similar to *glrbb* morphants co-injected with control morpholino showing that at the level of behavior *glrbb* is epistatic to *glra1*.

In addition, we also observed a novel morphological disruption in embryos co-injected with *glrbb*MOex5 and either *glra1*MOex4, or *glra1*MOex7 morpholinos but not in embryos co-injected with *glrbb*MOex5 and control morpholinos suggesting synergistic roles for *glra1* and *glrbb* in development, perhaps relating to their functional roles in spinal cord stem cells.

Table 3
Epistasis analysis between *glra1* and *glrbb* phenotypes. Batches of embryos were co-injected with either 0.5 mM *glrbb*MOex5 and 0.5 mM control morpholino, 0.5 mM *glrbb*MOex5 and 0.25 mM *glra1*MOex4, or 0.5 mM *glrbb*MOex5 and 0.5 mM *glra1*MOex7 and assayed for morphological and behavioral phenotypes between 28 and 36 hpf. Percentages of embryos, with numbers in each treatment in parentheses below, are indicated for each treatment and morphology. For behavior, larvae were tested for whether they ever produced accordion. The 'yes' for each treatment indicates that 'accordion' was the typical behavioral response.

	0.5 mM *glrbb*ex5 + 0.5 mM ConMO	0.5 mM *glrbb*ex5 + 0.25 mM *glra1*ex4	0.5 mM *glrbb*ex5 + 0.5 mM *glra1*ex7
Normal morphology	87% (n = 118)	9% (n = 5)	42% (n = 26)
Disrupted morphology	13% (n = 18)	91% (n = 52)	58% (n = 35)
Accordion?	Yes	Yes	Yes

Glycinergic synaptogenesis in control, glra1, and glrbb morphant zebrafish

To compare the impact of knocking down GlyR α1 and βb subunits on glycinergic synaptogenesis, we carried out immunohistochemistry, double-labeling 24 and 48 hpf fresh-frozen sections with antibodies recognizing GlyR α subunits and the GlyR clustering protein gephyrin (Fig. 7). At 24 and 48 hpf, progenitor cells are still actively dividing in the middle of the spinal cord; surrounding these progenitors are the first neurons to exit the cell cycle and differentiate. Differentiated neurons include primary motor neurons (PMNs) some interneurons, and Rohon Beard sensory neurons. For immunohistochemistry, we focus on the largest neurons, likely PMNs, in the motor neuron/interneuron domain (Fig. 7; white boxes). GlyR α and gephyrin immunohistochemistry were both characterized by bright puncta that likely reflect enrichment of these proteins at postsynaptic densities. Surprisingly, in 24 hpf control morphants, GlyR α subunit and gephyrin puncta did not co-localize (Figs. 7A & 8A). While gephyrin puncta were enriched exclusively in the domain occupied by differentiated neurons, the GlyR α subunit puncta also decorated progenitor cells in the medial cord (Fig. 7A; red arrowheads). Even within single neurons exhibiting both GlyR and gephyrin puncta, there was little overlap (Fig. 7A; red & green arrows).

In contrast to wild type embryos, when the GlyR α1 subunit was knocked down either using *glra1*MOex4 or *glra1*MOex7, GlyR puncta in the medial spinal cord were dramatically reduced (Figs. 7B & C). Remaining GlyR puncta were enriched in the lateral spinal cord where, in contrast to control morphants, more of the GlyR puncta co-localized with gephyrin (Figs. 7B, C & 8A *glra1*MOex4). As with GlyR α1 morphants, knocking down the GlyR βb subunit using *glrbb*MOex5 also reduces GlyR staining in the medial spinal cord. In addition, however, *glrbb* morphants also exhibited reduced GlyR α puncta in the lateral spinal cord with fewer puncta that co-localize with gephyrin (Fig. 7D). By 48 hpf in control morphants, GlyR and gephyrin puncta colocalized in the lateral spinal cord (Fig. 7A′). Knocking down the GlyR α1 subunit reduced the density of GlyR puncta (Figs. 7B′, C′ & 8B). Knocking down the GlyR βb subunit, as would be expected, also disrupted GlyR and gephyrin co-localization (Figs. 7D′ & 8B–C).

In summary, punctate GlyR immuno-staining was reduced in both *glra1* and *glrbb* morphants at both 24 and 48 hpf. At 24 hpf, GlyR puncta in *glra1* morphants were dramatically reduced in the medial spinal cord, although some remaining puncta – presumably containing other GlyR α subunits – co-localizing with gephyrin could be detected in the lateral spinal cord. This staining pattern contrasts with *glrbb* morphants, in which loss of both GlyR clusters and co-localization with gephyrin was evident.

Quantification of gene expression for components of the glycinergic synapse in developing zebrafish

To quantify the relative mRNA expression levels of genes known to be critical to glycinergic synapse function, we generated a developmental time-course for eleven zebrafish genes implicated in the function of glycinergic synapses using quantitative PCR (Fig. 9). While quantitative PCR yields no spatial information, it does reveal two distinct groupings of genes that share developmental expression trajectories. Expression of the majority of genes including *glra1*, *glra2*, *glra4a*, *glrba*, *glrbb*, *slc6a5* (GlyT2), and *gphnb* exhibited a steady increase with development. By contrast, expression of *glra3*, *slc6a9* (GlyT1) and *slc32a1* (VIAAT) increased until 48 hpf and then either leveled off (GlyT1/VIAAT) or decreased (*glra3*, *gphna*). These shared developmental expression trajectories could reflect shared transcriptional regulation. In the context of multiple duplicated subunits, qPCR also provides information about the dominant subunits expressed at different developmental time periods at the mRNA level. For example, in the case of the GlyR β subunits, the βb subunit mRNA is ~5 fold more abundant

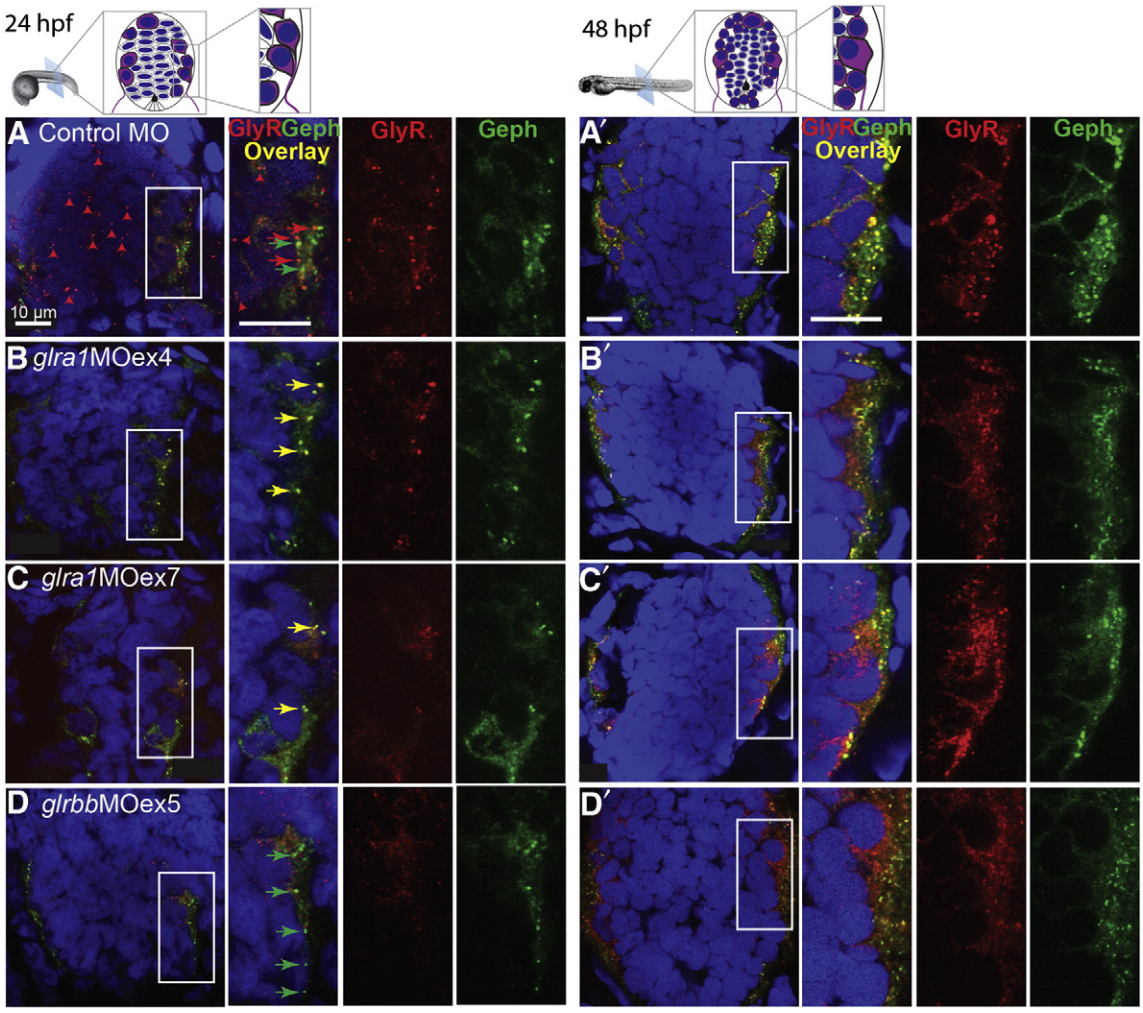

Fig. 7. GlyR α puncta are reduced in *glra1* morphants and absent in *glrbb* morphants. Transverse sections through fast-frozen 24 hpf (left; A–D) and 48 hpf (right; A′–D′) larvae were stained for GlyR α subunits (red), gephyrin (green), and nuclei (blue). Diagrams above the micrographs show the tight packing of spinal cord cells. In these diagrams, cells with purple cytoplasm represent the differentiated neurons: primary motor neurons (PMNs) that exit the spinal cord to innervate muscle, early differentiating interneurons, and dorsal sensory Rohon Beard neurons. These differentiated neurons form in a rind that surrounds the medial stem cells, outlined in gray. By 48 hpf more neurons have differentiated and become incorporated into the circuit as reflected by an increased synaptic staining on lateral neurons. Representative images for each stage and morpholino treatment are displayed as groupings of four images with the leftmost image giving a low magnification view of the entire spinal cord with the motor/inter-neuron region boxed in white magnified in the subsequent three images. A. In 24 hpf control morphants, GlyR α and gephyrin staining are non-overlapping. GlyR puncta decorate precursor cells near the spinal cord midline (red arrowheads) as well as lateral neurons (red arrows). Gephyrin puncta (green arrows) are solely associated with lateral neurons, but do not co-localize with GlyRs at this developmental time point. B, C. In both *glra1* morphants, GlyR α subunit staining is absent in precursors near the midline. Curiously, in *glra1* morphants, residual GlyR α subunits did co-localize with gephyrin (yellow arrows) in lateral neurons. D. In 24 hpf *glrbb*MOex5 morphants, gephyrin puncta (green arrows) occur in the absence of GlyR α subunit puncta. A′. In 48 hpf control morphants, GlyR α subunit and gephyrin puncta commonly co-localized. B′, C′. In 48 hpf *glra1* morphants, a subset of GlyR α subunit and gephyrin puncta commonly co-localized but these co-localized puncta are positioned more laterally than in control morphants. D′. 48 hpf *glrbb*MOex5 morphants lacked clear GlyR α subunit puncta, but exhibited smaller gephyrin puncta that tended towards the lateral neuropil rather than circum-nuclear as in control morphants. Scale bars: 10 µm.

at both 48 and 72 hpf than βa. Likewise, the expression of *gphna* mRNA dominates at 48 hpf being 35 times more abundant than *gphnb* while at 72 hpf, it is only four times more abundant. The levels of GlyR α subunit transcripts differ with the most abundant being *glra2* and *glra3*. Expression of *glra1*, *glra4a* and *glrbb*, is barely detectable at 24 and 32 hpf, but increases onwards from 48 hpf.

Discussion

Our study demonstrated that all available alleles of the GlyR mutant *bandoneon* correspond to defects in *glrbb*, encoding the GlyR βb subunit. Consistent with recent studies on human startle disease mutations in the GlyR β subunit gene (Al-Owain et al., 2012; Chung et al., 2013; James et al., 2013; Lee et al., 2013), mutations resulting in protein truncation are the predominant mechanism disrupting GlyR βb subunit function in the *beo* allele series (4/7 alleles), followed by missense mutations affecting residues in the membrane spanning domains M1/M2 (2/7 alleles) or large extracellular domain (1/7 alleles). Y79D introduces a negative charge and a hydrophilic residue into a packed area of hydrophobic side-chains, which is likely to disrupt the local β-sheet fold on which it resides in the extracellular domain, possibly indirectly affecting glycine binding. The substitution L255R may disrupt packing of hydrophobic and aromatic residues between TM helices due to the large, positively charged side-chain of arginine, thus affecting the correct fold of the subunit or insertion into the membrane. R275 is equivalent to R252 in the human GlyR α1 subunit (James et al., 2013). A spontaneous mutation causing the same substitution in this residue (R252H) is known to cause startle disease when inherited in compound heterozygote manner (Vergouwe et al., 1999). Substitutions at R252 in the GlyR α1 subunit have been shown to severely disrupt the correct function of

the protein, specifically affecting GlyR membrane trafficking (Rea et al., 2002). Thus, R275H in the zebrafish GlyR βb subunit is predicted to operate by a similar pathogenic mechanism.

Since mutations in GlyR α1, β subunit or GlyT2 genes all cause startle disease in dogs, cattle, mice and humans, one mystery is why no mutations in *glra1* or *slc6a5* have been discovered to date in phenotypic screens of zebrafish mutants generated by ENU mutagenesis (Granato et al., 1996). We now have a potential explanation for this finding, since knocking down *glra1* (encoding the GlyR α1 subunit) produced a relatively mild phenotype compared to *beo*, characterized by spasticity that delayed the onset of rhythmic motor behaviors. This phenotype is likely to be genuine, since it was reproduced using two different MOs, and using a dominant-negative zebrafish GlyR α1 subunit mutant, R270Q — equivalent to the most common dominant startle disease mutation found in humans (R271Q; Chung et al., 2010; Shiang et al., 1993).

Notably, this phenotype is distinct from the 'accordion' behavior produced by inactivation of *glrbb*, encoding the GlyR βb subunit (Hirata et al., 2005). While our study clearly implicates GlyRs containing the α1 subunit in the smooth transition from spontaneous coiling behaviors to propulsive locomotion, the finding that *glra1* loss-of-function causes this transient phenotype in zebrafish was unexpected. Several potential compensatory mechanisms have been observed in animals with loss-of-function mutations in the GlyR α1 subunit gene, including increased presynaptic glycine uptake, increased inhibitory GABAergic transmission, or up-regulation of additional GlyR α subunit genes (Graham et al., 2003; Gundlach et al., 1988; Kling et al., 1997; Lummis et al., 1990; Wässle et al., 1998). However, a strong visible phenotype is always observed in these animal models and in recessive human startle disease caused by *GLRA1* mutations (Chung et al., 2010). So what could be different in the zebrafish? Since the *beo* phenotype can also be reproduced by applying the GlyR antagonist strychnine (Granato et al., 1996; Hirata et al., 2005), our interpretation is that the *beo* phenotype results from the loss-of-function of multiple GlyR subtypes. This supported by epistasis experiments that demonstrate *glrbb* is epistatic to *glra1* at the level of behavior. Consistent with epistasis, immunohistochemistry showed that *glra1* morphants exhibited residual GlyR α subunit puncta, while in *glrbb* morphants, GlyR α subunits were trapped in intracellular aggregates. Moreover, qPCR results also identified *glra2*, *glra3*, and *glra4a* in developing embryos, which could participate in α2βb, α3βb or α4βb GlyRs. Certainly, compared with mammals, the zebrafish has additional opportunities for compensating for the loss of *glra1*, due to the duplication of the α4 subunit genes (*glra4a*, *glra4b*; Hirata et al., 2010). In our view, the zebrafish GlyR gene expansion (Hirata et al., 2010) reflects strong selective pressure

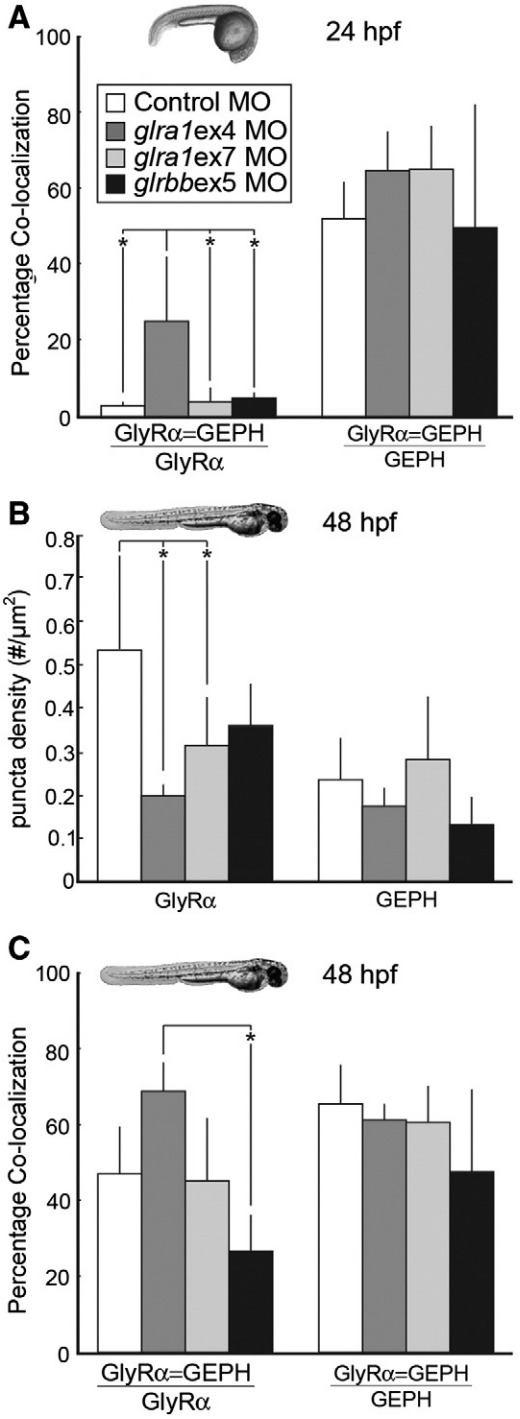

Fig. 8. GlyR densities are significantly reduced in *glra1* morphants, while the percentage of glycine receptors that co-localize with gephyrin is reduced in *glrbb* morphants. A. After GlyR α and gephyrin (GEPH) puncta were found using a customized MatLab program, co-localization was calculated in control (n = 7), *glra1* (ex4 n = 6; ex7 n = 3), and *glrbb* (n = 3) 24 hpf morphants in two ways: either as the fraction of GlyRs that co-localized with GEPH (ANOVA indicated a significant effect of morpholino injected on percent of GlyR α puncta that co-localizes with GEPH [$F(3,15) = 6.55$, $p = 0.005$]), or as the fraction of GEPH that colocalized with GlyR (ANOVA indicated no significant effect of morpholino injected [$F(3,15) = 1.27$, $p = 0.32$]). Bar graphs show means with error bars indicating standard deviation for all groups. Post hoc Bonferroni-corrected Student's t-tests compared all means and demonstrated that at $p < 0.05$ (* in graph), only *glra1*MOex4 had significantly more co-localization than control, *glra1*MOex7, and *glrbb*MOex5 morpholino treatments. Surprisingly fewer GlyR α puncta co-localize with GEPH at 24 hpf than at 48 hpf, C, while the proportion of GEPH colocalizing with GlyR puncta remains fairly constant. The proportion of GlyR α puncta that co-localize with GEPH is greatest in the *glra1*ex4 morphants that lack the GlyR α epitope, supporting the conclusion that in *glra1* morphants, residual co-localization reflects synaptic staining of GlyR α2, α3, or α4a. B. GlyR and GEPH densities were calculated in control (n = 6), *glra1* (ex4 n = 3; ex7 n = 7), and *glrbb* (n = 5) morphants at 48 hpf. Bar graphs show means with error bars indicating standard deviation. ANOVA indicates a significant effect of the mopholino injected on GlyR puncta density [$F(3, 16) = 4.39$, $p = 0.02$] but not on GEPH puncta [$F(3,16) = 2.03$, $p = 0.15$]. Post hoc Bonferroni-corrected Student's t-tests compared all means and demonstrated that at $p < 0.05$ (* in graph), only *glra1*MOex4 and *glra1*MOex7 were significantly reduced control morpholino treatments, although *glrbb*MOex5 treatments also trends in the same direction. C. Co-localization between GlyR and GEPH was quantified in control (n = 5), *glra1*(ex4 n = 3; ex7 n = 6), and *glrbb* (n = 4) 48 hpf larva in two ways: either as the fraction of GlyRs that co-localized with GEPH (ANOVA indicated a significant effect of morpholino injected on percent of GlyR α puncta that co-localizes with GEPH [$F(3,16) = 5.89$, $p = 0.007$]), or as the fraction of GEPH that colocalized with GlyR (ANOVA indicated no significant effect of morpholino injected [$F(3,14) = 1.56$, $p = 0.24$]). Bar graphs show means with error bars indicating standard deviation for all groups. Post hoc Bonferroni-corrected Student's t-tests compared all means and demonstrated that at $p < 0.05$ (* in graph), only the *glrbb*MOex5 treatment had significantly less co-localization than the *glra1*MOex4 treatment. In *glra1*MOex7 morphants, many peri-nuclear GlyR puncta fail to co-localize with GEPH. These likely represent GlyRs that are trapped intracellularly. Differences between *glra1*MOex4 and *glra1*MOex7 are likely explained by fewer intracellular GlyRs being recognized by mAb4a in *glra1*MOex4, since this antibody targets amino acids 96–105 that are lacking in *glra1*ex4 morphants. Therefore, residual staining in *glra1*MOex4 morphants is likely to reflect other GlyR α subunits, e.g. 2, 3, or 4a.

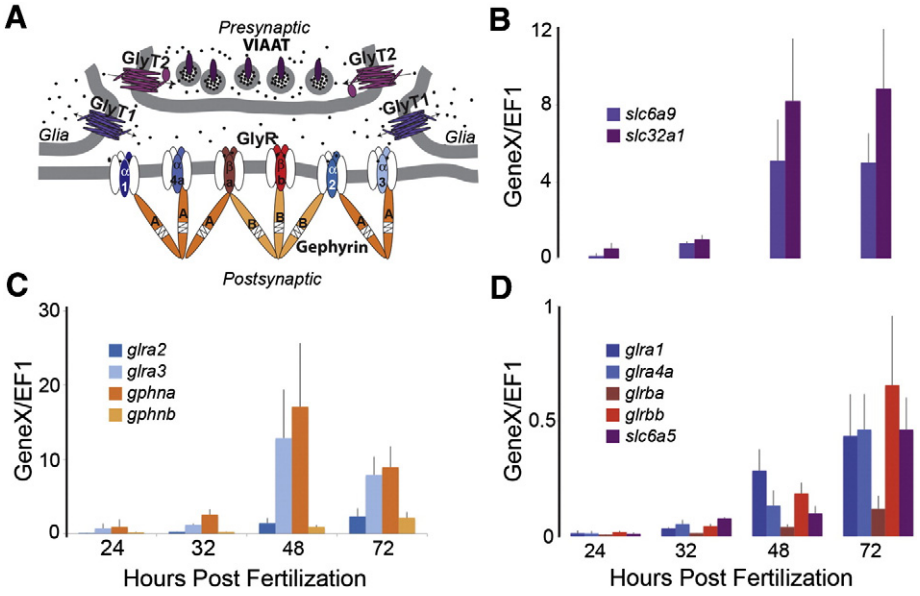

Fig. 9. Developmental expression profile of glycinergic synapse components. A. A schematic diagram of a glycinergic synapse depicts important proteins found in presynaptic, glial, and postsynaptic compartments. The functional classes of genes are color-coded with glycine transporters (GlyT1, GlyT2, VIAAT) in shades of purple, GlyR α1–4a and GlyR βa–b are red and blue respectively, and gephyrin A and B in shades of orange. GlyT2 transports glycine into the presynaptic terminal, where VIAAT loads glycine into vesicles for release into the synaptic cleft. Glycine then binds to postsynaptic GlyRs. Glycinergic signaling is terminated when glial GlyT1 removes glycine from the synaptic cleft. Six of the seven zebrafish GlyR subunits, α1, α3, α3, α4a, βa and βb, are shown assembled into pentameric, ligand-gated Cl^- channels with a 2α:3β subunit stoichiometry. These GlyRs are shown clustered at the synapse via interactions between GlyR β subunit and the scaffolding protein gephyrin. B–D. Average expression levels for all genes and time points (24, 32, 48, 72 hpf) are shown for an average of three independent mRNA preparations ± standard deviation. Genes are grouped into graphs according to their levels of expression and all gene expression is normalized to the housekeeping gene EF1. B. GlyT1 (*slc6a9*) and VIAAT (*slc32a1*) expression levels. C. GlyR α1, α4a, βa and βb subunit (*glra1*, *glra4a*, *glrba*, *glrbb*) and GlyT2 (*slc6a9*) expression levels. D. GlyR α2 subunit, α3 subunit, gephyrin-a and gephyrin-b (*glra2*, *glra3*, *gphna*, *gphnb*) expression levels.

for effective escape responses in this organism that develops externally with minimal parental care. Taken together, our data suggest that knocking down zebrafish orthologs of human hyperekplexia genes will likely produce a phenotypic range from more mild spasticity (*glra1* and *glrbb*) to bilateral contractions (*glrbb*).

The behavioral transition from slow coiling to fast rhythmic flexions (Saint-Amant and Drapeau, 1998; Warp et al., 2012), which is delayed in *glra1* morphants, reflects changes taking place in the connectivity of neural circuits. While embryonic slow coiling behaviors rely upon gap-junctional coupling among neurons (Brustein et al., 2003; Ganser and Dallman, 2009; Saint-Amant and Drapeau, 2001), larval rhythmic flexions rely upon synaptic inputs (Brustein et al., 2003; Kinkhabwala et al., 2011; Koyama et al., 2011; McLean and Fetcho, 2009; McLean et al., 2008). Our data show that zebrafish express α1βb GlyRs throughout this period of behavioral transition. These findings contrast with rodent spinal cord (Agaki et al., 1991; Becker et al., 1988; Harvey et al., 2004; Singer et al., 1998) and embryonic spinal cultures (Hoch et al., 1989) in which the GlyR α2 subunit predominates at early stages with the GlyR α1 and α3 subunits appearing postnatally. By contrast, in zebrafish, we show that GlyR α subunit immunostaining on neuronal precursors and differentiating neurons was disrupted by knocking down either *glra1* or *glrbb*, suggesting that the majority of early GlyR puncta in 24 hpf zebrafish spinal cord are composed of α1 and βb subunits.

In addition to glycine (Flint et al., 1998), non-synaptic release of both glutamate and GABA are known to cause Ca^{2+} transients in neural precursors that promote growth and maturation (Akerman and Cline, 2006; Ben-Ari and Spitzer, 2010; Haydar et al., 2000; Komuro and Rakic, 1996; Owens and Kriegstein, 2002). Both immature neurons and muscle express a variety of neurotransmitter receptors prior to innervation (Borodinsky et al., 2004; Moody and Bosma, 2005) at which point neurotransmitters influence a range of processes including proliferation, migration, and differentiation (Ben-Ari et al., 2007; LoTurco et al., 1995; Moody and Bosma, 2005; Owens and Kriegstein, 2002; Spitzer, 2006). For both glycine and GABA, the developmental transition from depolarizing to hyperpolarizing involves a shift in the chloride concentration gradient that is brought about by the up-regulation of the Cl^- transporter KCC2 (Ben-Ari et al., 2007). In zebrafish, prematurely expressing KCC2 to block the depolarizing influence of glycine and GABA reduces motor and interneuron differentiation (Reynolds et al., 2008). KCC2 expression is actually triggered by GABA-induced Ca^{2+} transients indicating a mechanism of developmental negative feedback (Fiumelli et al., 2005; Ganguly et al., 2001). Such feedback is likely a common feature of the developing nervous system (Dallman et al., 1998; Moody and Bosma, 2005) creating sequential checkpoints so that development only progresses when coordinate regulation of channels, receptors, and transporters successfully produce signals that feedback to promote maturation and qualitatively change excitability of the circuit (Ben-Ari and Spitzer, 2010). One possibility is that by knocking down *glra1* we delay the onset of rhythmic behaviors by disrupting signaling associated with depolarizing glycine (Ben-Ari and Spitzer, 2010).

Conclusions

Recent proteomic analyses of glutamatergic synapses suggest that up to a thousand proteins participate in this neuronal specialization (Grant, 2012). Even if glycinergic synapse function requires a fraction of this number of specialized proteins, the door is certainly open to complex forms of inheritance for startle disease. Despite the significant successes in identifying genetic defects that cause startle disease, many idiopathic cases remain in which the genetic cause is unresolved (Carta et al., 2012; Chung et al., 2010, 2013; James et al., 2013). Exome sequencing in these idiopathic cases will identify new candidate startle disease genes in the near future, necessitating animal models in which to test the validity of new candidate genes (Chung et al., 2013; James et al., 2013). Our study improves the utility of zebrafish as a startle disease model by identifying early phenotypes produced by two known startle disease genes in zebrafish that can be used to screen newly identified candidate genes via morpholino knockdown and

in overexpression models using proteins harboring potential disease-causing mutations.

Acknowledgments

We would like to thank UM Biology Molecular Core manager Dr. Hurt and Imaging Core manager Dr. Baker for their help with sequencing and confocal imaging respectively. We thank Drs. Baker and Wikramanayake for their feedback on writing, Anthony Sanchez for his assistance in analyzing embryonic movements, and Ricardo Cepeda (UM), Prof. Steve Wilson and Carole Wilson (UCL) for fish care. We would like to acknowledge Dr. Hiromi Hirata for his assistance in generating fast-frozen tissue sections and members of Dr. R. O. Wong's lab, a Travel Grant from the Company of Biologists, and Dr. Jiang for teaching Qing Yan to program MatLab to quantify immunohistochemistry. We also thank Lingyu Wang for assisting in the development of an image analysis work station. Grant/Other Support: Medical Research Council (G0601585 to RJH), University of Miami Provost Award and National Institutes of Health NINDS (K01NS048200 to JED).

Appendix A. Supplementary data

Supplementary data to this article can be found online at http://dx.doi.org/10.1016/j.nbd.2013.09.002.

References

Adzhubei, I.A., Schmidt, S., Peshkin, L., Ramensky, V.E., Gerasimova, A., Bork, P., Kondrashov, A.S., Sunyaev, S.R., 2010. A method and server for predicting damaging missense mutations. Nat. Methods 7, 248–249.

Agaki, H., Hirai, K., Hishinumu, F., 1991. Cloning of a glycine receptor subtype expressed in rat brain and spinal cord during a specific period of neuronal development. FEBS Lett. 281, 160–166.

Akerman, C.J., Cline, H.T., 2006. Depolarizing GABAergic conductances regulate the balance of excitation to inhibition in the developing retinotectal circuit *in vivo*. J. Neurosci. 26, 5117–5130.

Al-Owain, M., Colak, D., Al-Bakheet, A., Al-Hashmi, N., Shuaib, T., Al-Hemidan, A., Aldhalaan, H., Rahbeeni, Z., Al-Sayed, M., Al-Younes, B., Ozand, P.T., Kaya, N., 2012. Novel mutation in *GLRB* in a large family with hereditary hyperekplexia. Clin. Genet. 81, 479–484.

Becker, C.M., Hoch, W., Betz, H., 1988. Glycine receptor heterogeneity in rat spinal cord during postnatal development. EMBO J. 7, 3717–3726.

Ben-Ari, Y., Spitzer, N.C., 2010. Phenotypic checkpoints regulate neuronal development. Trends Neurosci. 33, 485–492.

Ben-Ari, Y., Gaiarsa, J.L., Tyzio, R., Khazipov, R., 2007. GABA: a pioneer transmitter that excites immature neurons and generates primitive oscillations. Physiol. Rev. 87, 1215–1284.

Borodinsky, L.N., Root, C.M., Cronin, J., Sann, S.B., Gu, X., Spitzer, N.C., 2004. Activity-dependent homeostatic specification of transmitter expression in embryonic neurons. Nature 429, 523–530.

Brustein, E., Saint-Amant, L., Buss, R.R., Chong, M., McDearmid, J.R., Drapeau, P., 2003. Step during the development of the zebrafish locomotor network. J. Physiol. Paris 97, 77–86.

Buckwalter, M.S., Cook, S.A., Davisson, M.T., White, W.F., Camper, S.A., 1994. A frameshift mutation in the mouse α1 glycine receptor gene (*Glra1*) results in progressive neurological symptoms and juvenile death. Hum. Mol. Genet. 3, 2025–2030.

Burgess, H.A., Granato, M., 2007. Sensorimotor gating in larval zebrafish. J. Neurosci. 27, 4984–4994.

Carta, E., Chung, S.-K., James, V.M., Robinson, A., Gill, J.L., Remy, N., Vanbellinghen, J.F., Drew, C.J.G., Cagdas, S., Cameron, D., Cowan, F.M., Del Toro, M.D., Graham, G.E., Manzur, A.Y., Masri, A., Rivera, S., Scalais, E., Shiang, R., Sinclair, K., Stuart, C.A., Tijssen, M.A.J., Wise, G., Zuberi, S.M., Harvey, K., Pearce, B.R., Topf, M., Thomas, R.H., Supplisson, S., Rees, M.I., Harvey, R.J., 2012. Mutations in the GlyT2 gene (*SLC6A5*) are a second major cause of hyperekplexia. J. Biol. Chem. 287, 28975–28985.

Charlier, C., Coppieters, W., Rollin, F., Desmecht, D., Agerholm, J.S., Cambisano, N., Carta, E., Dardano, S., Dive, M., Fasquelle, C., Frennet, J.C., Hanset, R., Hubin, X., Jorgensen, C., Karim, L., Kent, M., Harvey, K., Pearce, B.R., Simon, P., Tama, N., Nie, H., Vandeputte, S., Lien, S., Longeri, M., Fredholm, M., Harvey, R.J., Georges, M., 2008. Highly effective SNP-based association mapping and management of recessive defects in livestock. Nat. Genet. 40, 449–454.

Chung, S.K., Vanbellinghen, J.F., Mullins, J.G., Robinson, A., Hantke, J., Hammond, C.L., Gilbert, D.F., Freilinger, M., Ryan, M., Kruer, M.C., Masri, A., Gurses, C., Ferrie, C., Harvey, K., Shiang, R., Christodoulou, J., Andermann, F., Andermann, E., Thomas, R.H., Harvey, R.J., Lynch, J.W., Rees, M.I., 2010. Pathophysiological mechanisms of dominant and recessive *GLRA1* mutations in hyperekplexia. J. Neurosci. 30, 9612–9620.

Chung, S.K., Bode, A., Cushion, T.D., Thomas, R.H., Hunt, C., Wood, S.E., Pickrell, W.O., Drew, C.J., Yamashita, S., Shiang, R., Leiz, S., Longhardt, A.C., Raile, V., Weschke, B., Puri, R.D., Verma, I.C., Harvey, R.J., Ratnasinghe, D.D., Parker, M., Rittey, C., Masri, A., Lingappa, L., Howell, O.W., Vanbellinghen, J.F., Mullins, J.G., Lynch, J.W., Rees, M.I., 2013. *GLRB* is the third major gene of effect in hyperekplexia. Hum. Mol. Genet. 22, 927–940.

Dallman, J.E., Davis, A.K., Moody, W.J., 1998. Spontaneous activity regulates calcium-dependent K^+ current expression in developing ascidian muscle. J. Physiol. 511, 683–693.

Draper, B.W., Morcos, P.A., Kimmel, C.B., 2001. Inhibition of zebrafish *fgf8* pre-mRNA splicing with morpholino oligos: a quantifiable method for gene knockdown. Genesis 30, 154–156.

Eisen, J.S., Smith, J.C., 2008. Controlling morpholino experiments: don't stop making antisense. Development 135, 1735–1743.

Fiumelli, H., Cancedda, L., Poo, M.M., 2005. Modulation of GABAergic transmission by activity via postsynaptic Ca^{2+}-dependent regulation of KCC2 function. Neuron 48, 773–786.

Flint, A.C., Liu, X., Kriegstein, A.R., 1998. Nonsynaptic glycine receptor activation during early neocortical development. Neuron 20, 43–53.

Ganguly, K., Schinder, A.F., Wong, S.T., Poo, M.M., 2001. GABA itself promotes the developmental switch of neuronal GABAergic responses from excitation to inhibition. Neuron 105, 521–532.

Ganser, L.R., Dallman, J.E., 2009. Glycinergic synapse development, plasticity, and homeostasis in zebrafish. Front. Mol. Neurosci. 2, 30.

Gatto, C.L., Broadie, K., 2010. Genetic controls balancing excitatory and inhibitory synaptogenesis in neurodevelopmental disorder models. Front. Synaptic Neurosci. 2, 4.

Gill, J.L., Capper, D., Vanbellinghen, J.F., Chung, S.K., Higgins, R.J., Rees, M.I., Shelton, G.D., Harvey, R.J., 2011. Startle disease in Irish wolfhounds associated with a microdeletion in the glycine transporter GlyT2 gene. Neurobiol. Dis. 43, 184–189.

Giménez, C., Pérez-Siles, G., Martínez-Villarreal, J., Arribas-González, E., Jiménez, E., Núñez, E., de Juan-Sanz, J., Fernández-Sánchez, E., García-Tardón, N., Ibáñez, I., Romanelli, V., Nevado, J., James, V.M., Topf, M., Chung, S.K., Thomas, R.H., Desviat, L.R., Aragón, C., Zafra, F., Rees, M.I., Lapunzina, P., Harvey, R.J., López-Corcuera, B., 2012. A novel dominant hyperekplexia mutation Y705C alters trafficking and biochemical properties of the presynaptic glycine transporter GlyT2. J. Biol. Chem. 287, 28986–29002.

Graham, B.A., Schofield, P.R., Sah, P., Callister, R.J., 2003. Altered inhibitory synaptic transmission in superficial dorsal horn neurones in *spastic* and *oscillator* mice. J. Physiol. 551, 905–916.

Granato, M., van Eeden, F.J., Schach, U., Trowe, T., Brand, M., Furutani-Seiki, M., Haffter, P., Hammerschmidt, M., Heisenberg, C.P., Jiang, Y.J., Kane, D.A., Kelsh, R.N., Mullins, M.C., Odenthal, J., Nüsslein-Volhard, C., 1996. Genes controlling and mediating locomotion behavior of the zebrafish embryo and larva. Development 123, 399–413.

Grant, S.G.N., 2012. Synaptopathies: diseases of the synaptome. Curr. Opin. Neurobiol. 22, 522–529.

Gundlach, A.L., Dodd, P.R., Grabara, C.S., Watson, W.E., Johnston, G.A., Harper, P.A., Dennis, J.A., Healy, P.J., 1988. Deficit of spinal cord glycine/strychnine receptors in inherited myoclonus of Poll Hereford calves. Science 241, 1807–1810.

Harvey, R.J., Depner, U.B., Wässle, H., Ahmadi, S., Heindl, C., Reinold, H., Smart, T.G., Harvey, K., Schütz, B., Abo-Salem, O.M., Zimmer, A., Poisbeau, P., Welzl, H., Wolfer, D.P., Betz, H., Zeilhofer, H.U., Müller, U., 2004. GlyR α3: an essential target for spinal PGE_2-mediated inflammatory pain sensitization. Science 304, 884–887.

Harvey, R.J., Topf, M., Harvey, K., Rees, M.I., 2008. The genetics of hyperekplexia: more than startle! Trends Genet. 24, 439–447.

Haydar, T.F., Wang, F., Schwartz, M.L., Rakic, P., 2000. Differential modulation of proliferation in the neocortical ventricular and subventricular zones. J. Neurosci. 20, 5764–5774.

Hirata, H., Saint-Amant, L., Downes, G.B., Cui, W.W., Zhou, W., Granato, M., Kuwada, J.Y., 2005. Zebrafish bandoneon mutants display behavioral defects due to a mutation in the glycine receptor β-subunit. Proc. Natl. Acad. Sci. U. S. A. 102, 8345–8350.

Hirata, H., Carta, E., Yamanaka, I., Harvey, R.J., Kuwada, J.Y., 2010. Defective glycinergic synaptic transmission in zebrafish motility mutants. Front. Mol. Neurosci. 2, 26.

Hoch, W., Betz, H., Becker, C.M., 1989. Primary cultures of mouse spinal cord express the neonatal isoform of the inhibitory glycine receptor. Neuron 3, 339–348.

Holland, K.D., Fleming, M.T., Cheek, S., Moran, J.L., Beier, D.R., Meisler, M.H., 2006. *De novo* exon duplication in a new allele of mouse *Glra1* (*spasmodic*). Genetics 174, 2245–2247.

Hurley, I.A., Mueller, R.L., Dunn, K.A., Schmidt, E.J., Friedman, M., Ho, R.K., Prince, V.E., Yang, Z., Thomas, M.G., Coates, M.I., 2007a. A new time-scale for ray-finned fish evolution. Proc. Biol. Sci. 274, 489–498.

Hurley, I.A., Scemama, J.L., Prince, V.E., 2007b. Consequences of *hoxb1* duplication in teleost fish. Evol. Dev. 9, 540–554.

James, V.M., Bode, A., Chung, S.K., Gill, J.L., Nielsen, M., Cowan, F.M., Vujic, M., Thomas, R.H., Rees, M.I., Harvey, K., Keramidas, A., Topf, M., Ginjaar, I., Lynch, J.W., Harvey, R.J., 2013. Novel missense mutations in the glycine receptor β subunit gene (*GLRB*) in startle disease. Neurobiol. Dis. 52, 137–149.

Kimmel, C.B., Ballard, W.W., Kimmel, S.R., Ullmann, B., Schilling, T.F., 1995. Stages of embryonic development of the zebrafish. Dev. Dyn. 203, 253–310.

Kingsmore, S.F., Giros, B., Suh, D., Bieniarz, M., Caron, M.G., Seldin, M.F., 1994. Glycine receptor β-subunit gene mutation in *spastic* mouse associated with LINE-1 element insertion. Nat. Genet. 7, 136–141.

Kinkhabwala, A., Riley, M., Koyama, M., Monen, J., Satou, C., Kimura, Y., Higashijima, S., Fetcho, J., 2011. A structural and functional ground plan for neurons in the hindbrain of zebrafish. Proc. Natl. Acad. Sci. U. S. A. 108, 1164–1169.

Kling, C., Koch, M., Saul, B., Becker, C.M., 1997. The frameshift mutation *oscillator* ($Glra1^{spd\text{-}ot}$) produces a complete loss of glycine receptor α1-polypeptide in mouse central nervous system. Neuroscience 78, 411–417.

Komuro, H., Rakic, P., 1996. Intracellular Ca^{2+} fluctuations modulate the rate of neuronal migration. Neuron 17, 275–285.
Koyama, M., Kinkhabwala, A., Satou, C., Higashijima, S., Fetcho, J., 2011. Mapping a sensory–motor network onto a structural and functional ground plan in the hindbrain. Proc. Natl. Acad. Sci. U. S. A. 108, 1170–1175.
Kumar, P., Henikoff, S., Ng, P.C., 2009. Predicting the effects of coding non-synonymous variants on protein function using the SIFT algorithm. Nat. Protoc. 4, 1073–1081.
Lee, C.G., Kwon, M.J., Yu, H.J., Nam, S.H., Lee, J., Ki, C.S., Lee, M., 2013. Clinical features and genetic analysis of children with hyperekplexia in Korea. J. Child Neurol. 28, 90–94.
LoTurco, J.J., Owens, D.F., Heath, M.J.S., Davis, M.B.E., Kriegstein, A.R., 1995. GABA and glutamate depolarize cortical progenitor cells and inhibit DNA synthesis. Neuron 15, 1287–1298.
Lummis, S.C., Gundlach, A.L., Johnston, G.A., Harper, P.A., Dodd, P.R., 1990. Increased γ-aminobutyric acid receptor function in the cerebral cortex of myoclonic calves with an hereditary deficit in glycine/strychnine receptors. J. Neurochem. 55, 421–426.
Lynch, J.W., 2004. Molecular structure and function of the glycine receptor chloride channel. Physiol. Rev. 84, 1051–1095.
McLean, D.L., Fetcho, J.R., 2009. Spinal interneurons differentiate sequentially from those driving the fastest swimming movements in larval zebrafish to those driving the slowest ones. J. Neurosci. 29, 13566–13577.
McLean, D.L., Masino, M.A., Koh, I.Y., Lindquist, W.B., Fetcho, J.R., 2008. Continuous shifts in the active set of spinal interneurons during changes in locomotor speed. Nat. Neurosci. 11, 1419–1429.
Moody, W.J., Bosma, M.M., 2005. Ion channel development, spontaneous activity, and activity-dependent development in nerve and muscle cells. Physiol. Rev. 85, 883–941.
Morgan, J.L., Schubert, T., Wong, R.O., 2008. Developmental patterning of glutamatergic synapses onto retinal ganglion cells. Neural Dev. 3, 8.
Mülhardt, C., Fischer, M., Gass, P., Simon-Chazottes, D., Guénet, J.L., Kuhse, J., Betz, H., Becker, C.M., 1994. The *spastic* mouse: aberrant splicing of glycine receptor β subunit mRNA caused by intronic insertion of L1 element. Neuron 13, 1003–1015.
Ogino, K., Ramsden, S.L., Keib, N., Schwarz, G., Harvey, R.J., Hirata, H., 2011. Duplicated gephyrin genes showing distinct tissue distribution and alternative splicing patterns mediate molybdenum cofactor biosynthesis, glycine receptor clustering, and escape behavior in zebrafish. J. Biol. Chem. 286, 806–817.
Owens, D.F., Kriegstein, A.R., 2002. Developmental neurotransmitters? Neuron 36, 989–991.
Pierce, K.D., Handford, C.A., Morris, R., Vafa, B., Dennis, J.A., Healy, P.J., Schofield, P.R., 2001. A nonsense mutation in the α1 subunit of the inhibitory glycine receptor associated with bovine myoclonus. Mol. Cell. Neurosci. 17, 354–363.
Rea, R., Tijssen, M.A., Herd, C., Frants, R.R., Kullmann, D.M., 2002. Functional characterisation of compound heterozygosity for GlyR α1 mutations in the startle disease hyperekplexia. Eur. J. Neurosci. 16, 186–196.
Rees, M.I., Lewis, T.M., Kwok, J.B., Mortier, G.R., Govaert, P., Snell, R.G., Schofield, P.R., Owen, M.J., 2002. Hyperekplexia associated with compound heterozygote mutations in the β-subunit of the human inhibitory glycine receptor (*GLRB*). Hum. Mol. Genet. 11, 853–860.
Rees, M.I., Harvey, K., Pearce, B.R., Chung, S.K., Duguid, I.C., Thomas, P., Beatty, S., Graham, G.E., Armstrong, L., Shiang, R., Abbott, K.J., Zuberi, S.M., Stephenson, J.B., Owen, M.J., Tijssen, M.A., van den Maagdenberg, A.M., Smart, T.G., Supplisson, S., Harvey, R.J., 2006. Mutations in the gene encoding GlyT2 (*SLC6A5*) define a presynaptic component of human startle disease. Nat. Genet. 38, 801–806.
Reynolds, A., Brustein, E., Liao, M., Mercado, A., Babilonia, E., Mount, D.B., Drapeau, P., 2008. Neurogenic role of the depolarizing chloride gradient revealed by global overexpression of KCC2 from the onset of development. J. Neurosci. 28, 1588–1597.
Rozen, S., Skaletsky, H.J., 2000. Primer3 on the WWW for general users and for biologist programmers. In: Krawetz, S., Misener, S. (Eds.), Bioinformatics Methods and Protocols: Methods in Molecular Biology. Humana Press, Totowa, NJ, pp. 365–386.
Ryan, S.G., Buckwalter, M.S., Lynch, J.W., Handford, C.A., Segura, L., Shiang, R., Wasmuth, J.J., Camper, S.A., Schofield, P., O'Connell, P., 1994. A missense mutation in the gene encoding the α1 subunit of the inhibitory glycine receptor in the *spasmodic* mouse. Nat. Genet. 7, 131–135.
Saint-Amant, L., Drapeau, P., 1998. Time course of the development of motor behaviors in the zebrafish embryo. J. Neurobiol. 37, 622–632.
Saint-Amant, L., Drapeau, P., 2001. Synchronization of an embryonic network of identified spinal interneurons solely by electrical coupling. Neuron 31, 1035–1046.
Shiang, R., Ryan, S.G., Zhu, Y.Z., Hahn, A.F., O'Connell, P., Wasmuth, J.J., 1993. Mutations in the α1 subunit of the inhibitory glycine receptor cause the dominant neurologic disorder, hyperekplexia. Nat. Genet. 5, 351–358.
Singer, J.H., Talley, E.M., Bayliss, D.A., Berger, A.J., 1998. Development of glycinergic synaptic transmission to rat brain stem motoneurons. J. Neurophysiol. 80, 2608–2620.
Soto, F., Bleckert, A., Lewis, R., Kang, Y., Kerschensteiner, D., Craig, A.M., Wong, R.O., 2011. Coordinated increase in inhibitory and excitatory synapses onto retinal ganglion cells during development. Neural Dev. 6, 31.
Spitzer, N.C., 2006. Electrical activity in early neuronal development. Nature 444, 707–712.
Tang, R., Dodd, A., Lai, D., McNabb, W.C., Love, D.R., 2007. Validation of zebrafish (*Danio rerio*) reference genes for quantitative real-time RT-PCR normalization. Acta Biochim. Biophys. Sin. 3, 384–390.
Thomas, R.H., Stephenson, J.B.P., Harvey, R.J., Rees, M.I., 2010. Hyperekplexia: stiffness, startle and syncope. J. Pediatr. Neurol. 8, 11–14.
Traka, M., Seburn, K.L., Popko, B., 2006. *Nmf11* is a novel ENU-induced mutation in the mouse glycine receptor α1 subunit. Mamm. Genome 17, 950–955.
Vergouwe, M.N., Tijssen, M.A., Peters, A.C., Wielaard, R., Frants, R.R., 1999. Hyperekplexia phenotype due to compound heterozygosity for *GLRA1* gene mutations. Ann. Neurol. 46, 634–638.
Warp, E., Agarwal, G., Wyart, C., Friedmann, D., Oldfield, C.S., Conner, A., Del Bene, F., Arrenberg, A.B., Baier, H., Isacoff, E.Y., 2012. Emergence of patterned activity in the developing zebrafish spinal cord. Curr. Biol. 22, 93–102.
Wässle, H., Koulen, P., Brandstätter, J.H., Fletcher, E.L., Becker, C.M., 1998. Glycine and GABA receptors in the mammalian retina. Vision Res. 38, 1411-1130.